minerals

MDPI

Article

Provenance Inheritance and Adjustment of the Silurian Kepingtag Formation in the Tarim Basin: Constraints from Detrital Zircon U–Pb Geochronology and Geological Implications

Qiyuan Zhang [1], Xiang Zhang [2,*] and Jingchun Tian [2]

[1] College of Earth and Planetary Sciences, Chengdu University of Technology, Chengdu 610059, China; zqy1991862492@163.com
[2] Institute of Sedimentary Geology, Chengdu University of Technology, Chengdu 610059, China; tjc@cdut.edu.cn
* Correspondence: zhangxiang06@cdut.edu.cn

Abstract

The Early Silurian Kepingtag Formation in the Tarim Basin records changes in sediment supply during a major tectonic transition. However, the extent of provenance inheritance and differentiation between its lower and upper sandstone members remains poorly constrained. In this study, detrital zircon U–Pb geochronological analyses were conducted on two sandstone samples collected from the Dawangou section along the northwestern margin of the Tarim Basin, yielding 150 concordant ages. These new data were integrated with previously published detrital zircon age spectra and regional tectonic and paleogeomorphic evidence to investigate provenance evolution within the Kepingtag Formation. Regional comparisons of detrital zircon age spectra across the Tarim Basin reveal three characteristic age clusters: 1100–700 Ma, 2000–1600 Ma, and 600–400 Ma. The lower sandstone member is dominated by Neoproterozoic age populations, with major peaks at approximately 750 and 994 Ma. The upper sandstone member retains prominent Neoproterozoic-age populations, with major peaks at approximately 762 and 813 Ma, accompanied by a minor Early Paleozoic detrital zircon component indicating a younger provenance signature. Sediment supply during deposition of the lower sandstone member was predominantly derived from erosion of inherited Precambrian paleo-uplifts within the basin, accompanied by locally substantial Early Paleozoic detrital input in eastern Tarim. During deposition of the upper sandstone member, the 1100–700 Ma age population remained prominent, whereas Early Paleozoic age signatures became markedly more pronounced in the northern and eastern regions of the basin. These characteristics suggest that Precambrian basement rocks and recycled sedimentary cover sequences continuously supplied detrital material throughout deposition of the Kepingtag Formation, with additional, spatially variable contributions from active tectonic belts along the basin margins, particularly the Altun Orogenic Belt and the active tectonic belts along the northern margin of the Tarim Basin. This interpretation is supported by the data in this study, although the relative contributions and temporal variations in individual source regions remain to be further constrained. Overall, provenance evolution of the Kepingtag Formation was characterized by stage-dependent adjustments superimposed on a persistent inherited provenance framework, reflecting sustained sediment contributions from Precambrian basement sources and spatially and temporally variable inputs from surrounding active orogenic belts.

Check for updates

Academic Editors: Georgia Pe-Piper and Zhenhong Li

Received: 20 October 2026
Revised: 10 November 2026
Accepted: 13 November 2026
Published: 16 November 2026

Copyright: © 2026 by the authors. Licensee MDPI, Basel, Switzerland. This article is an open access article distributed under the terms and conditions of the Creative Commons Attribution (CC BY) license.

Keywords: Tarim Basin; Kepingtag Formation; detrital zircon U-Pb geochronology; provenance analysis

1. Introduction

The Tarim Basin, located between the Paleo-Asian and Tethyan tectonic domains, is a large superimposed sedimentary basin that has undergone multiple episodes of tectonic and sedimentary evolution [1–3]. The Late Ordovician–Early Silurian marked a period of significant tectonic reorganization in the Tarim Basin during the Early Paleozoic, when tectonic activity along the surrounding orogenic belts and the differential evolution of inherited intracratonic paleo-uplifts jointly influenced the basin's paleogeomorphic configuration, sediment supply, and depositional system development [4]. In contrast to widespread marine carbonate deposition during the Ordovician, terrigenous clastic sedimentation expanded considerably during the Silurian, reflecting a major transition in the tectono-sedimentary setting of the basin. The Lower Silurian Kepingtag Formation, which extensively overlies a regional unconformity developed on the Ordovician strata, provides an important stratigraphic record for investigating the Late Ordovician–Early Silurian tectonic transition and provenance evolution [5]. It also represents a significant target for hydrocarbon exploration in the Tarim Basin [6].

Previous studies have investigated the provenance and tectonic setting of the Kepingtag Formation using sandstone petrography, geochemistry, heavy mineral assemblages, and detrital zircon U–Pb geochronology, leading to different interpretations of its sediment sources. Based on sandstone elemental geochemistry, Wang et al. [7] examined the provenance and tectonic setting of Silurian sandstones in the central Tarim Basin and suggested that the sediments were mainly derived from recycled orogenic sources and felsic igneous rocks. Using detrital zircon U–Pb age data from the Lower Silurian succession in the Keping area, Niu et al. [8] investigated the provenance and source-rock ages of the Kepingtag Formation in the northern Tarim Basin, highlighting the contributions of the Tabei Paleo-uplift and its associated basement rocks. Li et al. [9] subsequently examined the provenance characteristics of the Kepingtag Formation in the central Tarim Basin based on detrital zircon U–Pb age data. By integrating heavy mineral assemblages and detrital zircon geochronology, Guo et al. [10] suggested that, in addition to sustained sediment supply from intracratonic paleo-uplifts, the Silurian deposits in the Keping area may also have received detrital material from the northern margin of the Tarim Craton and the West Kunlun Orogenic Belt. Zhong et al. [11] compared detrital zircon age spectra from Ordovician–Silurian strata, identified regional variations in provenance composition across the northwestern Tarim Basin, and discussed the relationship between Early Paleozoic zircon populations and tectonic evolution along the northern basin margin.

Collectively, these studies indicate that the Kepingtag Formation was characterized by a complex, multi-source provenance system, potentially involving contributions from inherited Precambrian basement sources within the basin and the surrounding active orogenic belts. Although previous studies have provided important insights into the potential source areas and tectonic setting of the Kepingtag Formation, detrital zircon geochronological investigations have largely focused on individual regions, such as Keping, northern Tarim, and central Tarim, and systematic comparisons of the spatial variations in detrital zircon age spectra remain limited. Furthermore, the different lithologic members of the Kepingtag Formation record distinct stages of evolution in the basin's depositional environments and paleogeomorphic configuration. However, the inheritance of detrital zircon age populations between the lower and upper sandstone members, as well as their regional variations, has

not been systematically evaluated through statistical comparisons. Therefore, correlations between detrital zircon age peaks and tectonothermal events in the surrounding orogenic belts alone are insufficient to fully explain provenance adjustments during successive depositional stages. An integrated analysis combining the geochronological characteristics of potential source areas, stratigraphic architecture, and regional paleogeomorphic framework is thus necessary to better constrain provenance evolution in the Kepingtag Formation.

Detrital zircon U–Pb geochronology has become a well-established and reliable approach for provenance analysis and reconstructing tectonic evolution [7–10]. Accordingly, two sandstone samples (DWG-KP1 and DWG-KP5) were collected from the lower and upper sandstone members of the Kepingtag Formation at the Dawangou section along the northwestern margin of the Tarim Basin. Detrital zircons were subjected to cathodoluminescence (CL) imaging and LA-ICP-MS U–Pb dating, yielding 150 concordant ages from 164 analytical spots. In addition, previously published detrital zircon U–Pb age datasets from different tectonic units and lithologic members of the Kepingtag Formation across the eastern, southern, and northern Tarim Basin were systematically compiled. By analyzing detrital zircon age distributions and integrating the geochronological characteristics of potential source areas, regional tectonic settings, stratigraphic relationships, and paleogeomorphic features, this study focuses on three key aspects: (1) the spatial differentiation of detrital zircon age spectra and potential source areas of the Kepingtag Formation; (2) provenance inheritance and stage-dependent adjustment between the lower and upper sandstone members; and (3) the potential influences of peripheral orogenic activity and intracratonic paleogeomorphic changes on provenance evolution. The findings are expected to provide new insights into Early Silurian provenance evolution in the Tarim Basin and its broader regional geological implications.

2. Geological Setting

The Tarim Basin is located in the Xinjiang Uygur Autonomous Region of northwestern China (Figure 1b). It extends predominantly east–west, measuring approximately 1400 km from east to west and 550 km from north to south, and covers an area of approximately 5.6×10^5 k^{22}. The basin is bounded by the Tianshan Mountains to the north, the West Kunlun Mountains to the west, and the Altun Mountains to the east [1,2,12,13]. The Tarim Basin is underlain by a relatively stable Precambrian crystalline basement, which is overlain by Mesoproterozoic–Neoproterozoic to Phanerozoic marine and continental sedimentary successions. These geological records document a prolonged tectonic evolution involving craton formation, continental rifting, passive continental margin development, and subsequent basin reorganization under the influence of surrounding orogenic processes [7,14].

Based on differences in basement characteristics, sedimentary filling patterns, structural deformation styles, and regional tectonic evolution, various tectonic subdivision schemes have been proposed for the Tarim Basin. In this study, the tectonic subdivision scheme established by the Northwest Oilfield Company of Sinopec was adopted. The basin margins are characterized by peripheral uplift zones, including the Keping Uplift Belt, Tiekelike Uplift Belt, Kuruktag Uplift, and Altun Uplift Belt. The basin interior is subdivided into 13 first-order tectonic units, of which nine are distributed within the Silurian depositional area. These comprise two depressions, two slopes, and five uplifts: the Manjiaer and Awati depressions; the Maigaiti and Kongquehe slopes; and the Tabei Uplift, Tazhong Uplift, Bachu Uplift, Shuntuoguole Low Uplift, and Tadong Uplift (Figure 1a). Owing to the multiple episodes of tectonic evolution experienced by the Tarim Basin, these tectonic units have undergone distinct tectono-sedimentary histories, resulting in complex structural and stratigraphic architectures [15–17].

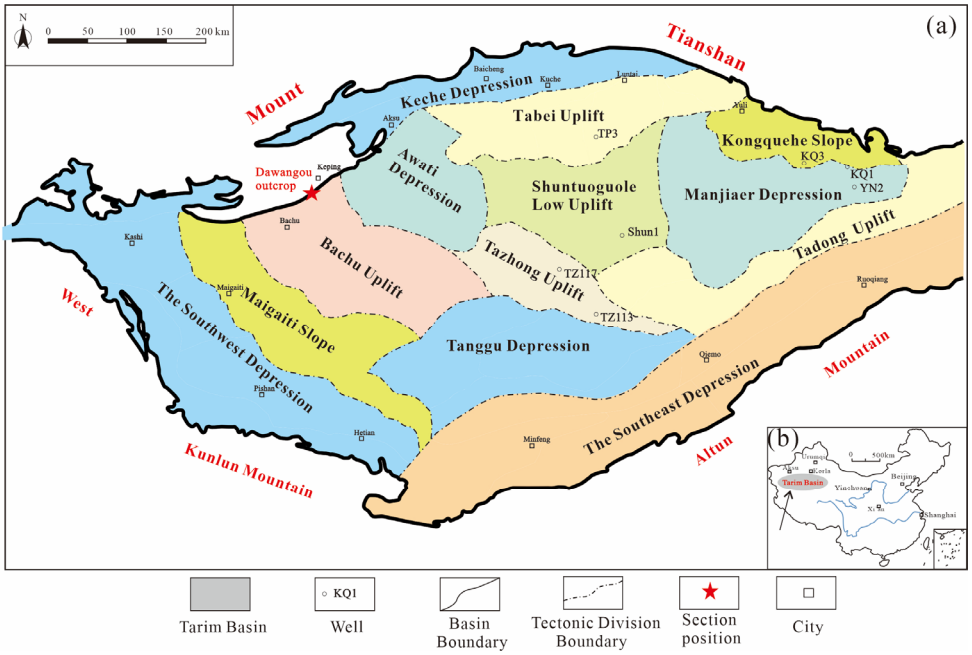


Figure 1. (**a**) The tectonic units of the Tarim Basin with the Keping study area and Tabei Uplift in red box. (**b**) Regional location map of the Tarim Basin.

The Kepingtag Formation in the study area is subdivided into three members in ascending order: the lower sandstone member (S_1k^1), middle mudstone member (S_1k^2), and upper sandstone member (S_1k^3) (Figure 2). This formation exhibits conformable contact with the overlying Tataertag Formation and parallel unconformity with the underlying Yingan or Qilang Formation. The Tataertag Formation is predominantly composed of interbedded purplish-red mudstones and argillaceous siltstones. The Yingan Formation consists of a suite of black mudstone deposits. The Qilang Formation developed a set of gray marls.

Based on Silurian drilling data and previous stratigraphic studies, this study adopted the stratigraphic subdivision scheme established by the Northwest Oilfield Company of Sinopec. The Kepingtag Formation is assigned to the Early Silurian and is lithologically subdivided into three members, characterized by an overall coarse–fine–coarse depositional succession (Figure 2). In ascending stratigraphic order, these comprise the lower sandstone member (S_1k^1), middle mudstone member (S_1k^2), and upper sandstone member (S_1k^3). The lower sandstone member consists predominantly of grayish-green to dark-gray quartz sandstones and lithic sandstones interbedded with siltstones and argillaceous siltstones. The sandstones commonly exhibit parallel bedding, low-angle cross-bedding, and wedge-shaped cross-bedding, with trough cross-bedding also observed in outcrop sections. The middle mudstone member is mainly composed of light-gray mudstones and grayish-green siltstones interbedded with argillaceous siltstones. The upper sandstone member consists primarily of green to grayish-green fine-grained sandstones and quartz-rich lithic sandstones, with grain sizes predominantly ranging from fine to medium sand [18,19]. Based on lithological characteristics and stratigraphic architecture, the Kepingtag Formation exhibits two distinct vertical succession patterns: two-member and three-member successions. The two-member succession comprises the middle mudstone and upper sandstone members, with the lower sandstone member absent, and is mainly distributed in the central Tarim region. In contrast, the three-member succession consists of the lower sandstone, middle mudstone, and upper sandstone members and is more widely developed, particularly in the Manjiaer, eastern Tarim, and Shunbei areas. In the Tabei region, the middle and upper portions of the upper

sandstone member are locally absent due to subsequent erosional truncation, as exemplified by Well TP2. The spatial distribution and stratigraphic absence of these members reflect the pre-Silurian uplift–depression configuration of the basin, as well as the effects of subsequent tectonic uplift and erosion (Figure 2).

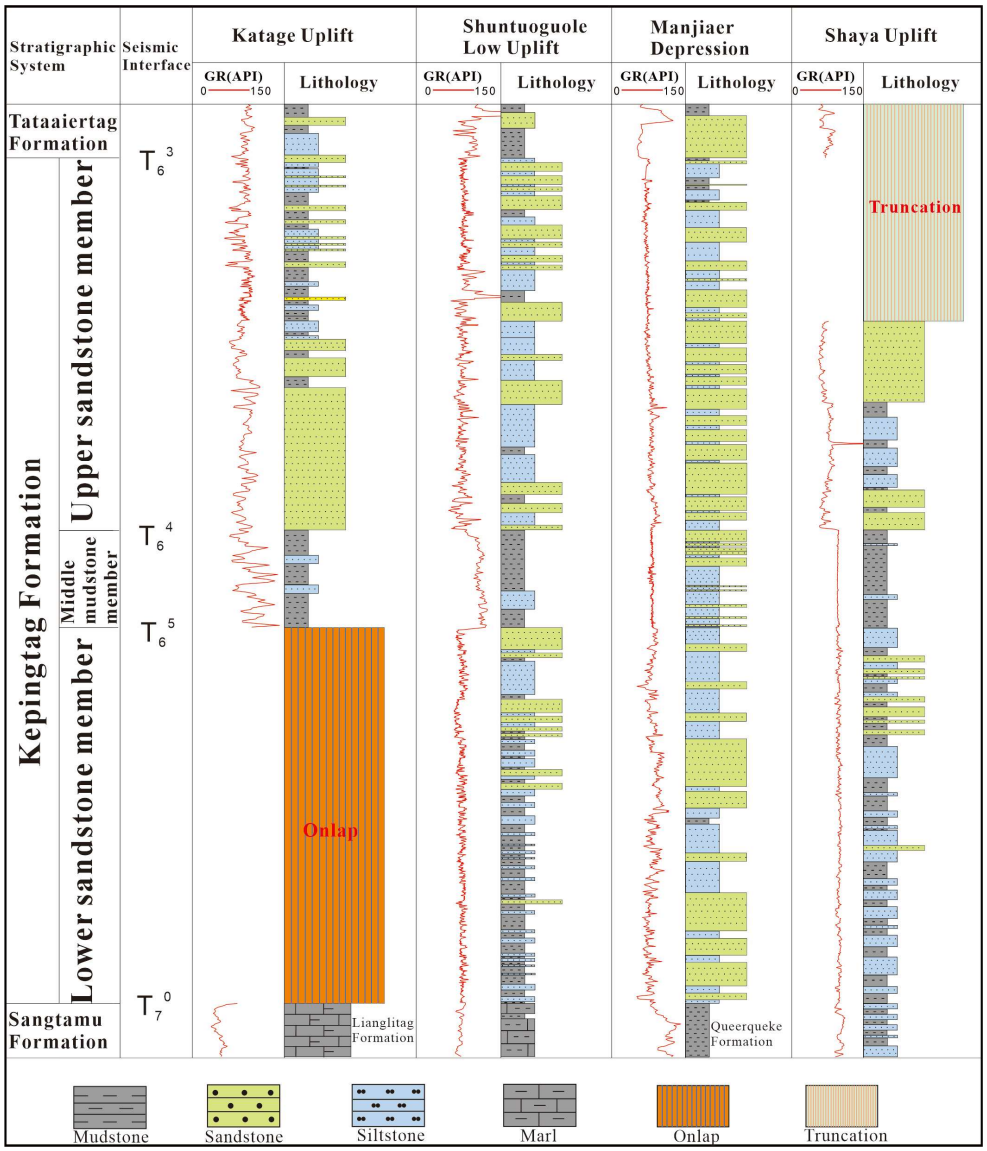


Figure 2. Stratigraphic framework map of the Kepingtag Formation (modified after [18]).

3. Materials and Methods

3.1. Zircon U-Pb Geochronology

The Dawangou section, located along the northwestern margin of the Tarim Basin, is a well-established reference section for the Ordovician–Silurian succession. The strata are continuously exposed and well preserved, with abundant sedimentary structures, making this section particularly important for investigating the field characteristics of the Silurian Kepingtag Formation, reconstructing tectonic activities along the basin margins, and understanding regional sedimentary evolution. The section is situated in the northwestern part of the Tarim Basin, approximately 75 km southwest of Aksu City and 15 km northwest of Yingan Village (Figure 3a). The starting point of the section is located at 78°29′6.72″ E, 41°53′24.6″ N, at an elevation of approximately 1762 m.

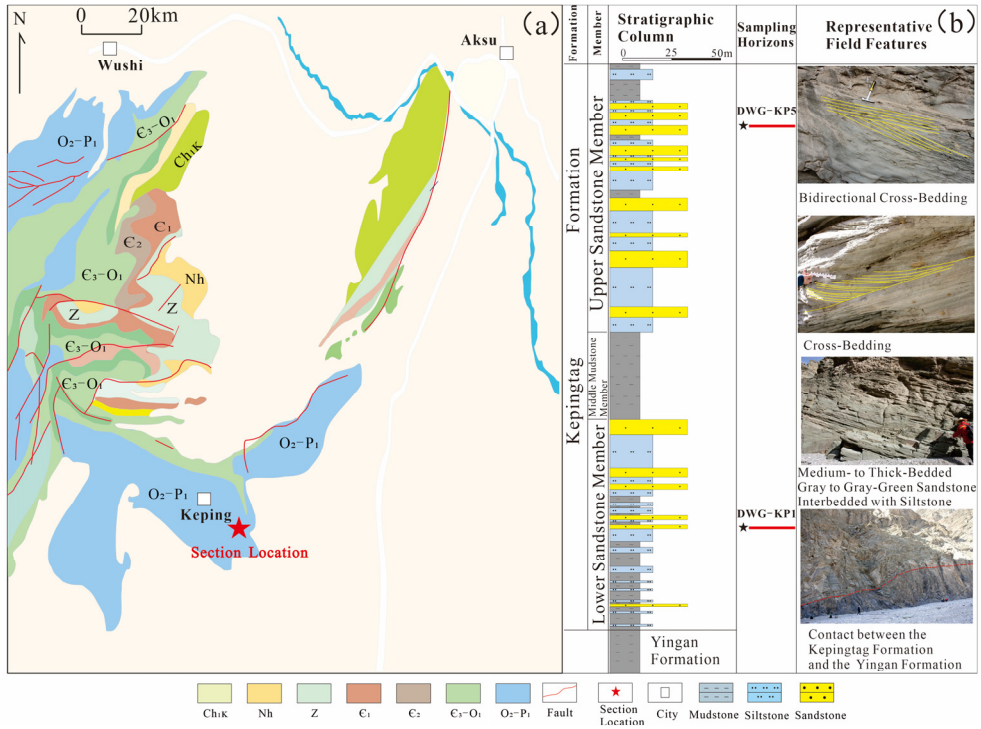


Figure 3. Location, regional geological setting, stratigraphic characteristics, and representative field features of the Dawangou section in the Tarim Basin. (**a**) Location and regional geological map of the Dawangou section; (**b**) stratigraphic column of the Kepingtag Formation showing sampling horizons and representative field features.

The upper sandstone member of the Kepingtag Formation consists predominantly of interbedded gray-green sandstone and gray-black mudstone, with gray-green medium-grained sandstone occurring at the top, and has an overall thickness of approximately 160 m. The lower sandstone member is composed mainly of gray-green medium-grained sandstone and interbedded gray-green mudstone and sandstone, with a total thickness of approximately 100 m. The Kepingtag Formation unconformably overlies the black shale of the Upper Ordovician Yingan Formation, with a recognizable unconformity surface and an underlying paleoweathering crust. Typical sedimentary structures are well developed in the section, including bidirectional cross-bedding indicative of tidal-current activity, suggesting that the succession was deposited predominantly in a tidal-flat environment (Figure 3b).

To better investigate provenance differences between the lower and upper sandstone members of the Kepingtag Formation, two sandstone samples were collected from the corresponding stratigraphic intervals at the Dawangou section. Sample DWG-KP1 was collected from the lower sandstone member at 78°29′6.72″ E, 41°53′24.6″ N, with an elevation of 1739.8 m, and is classified as lithic sandstone. Sample DWG-KP5 was collected from the upper sandstone member at 78°29′8.74″ E, 41°53′36.6″ N, with an elevation of 1740.3 m, and is also classified as lithic sandstone. Each sample weighed approximately 2 kg.

Zircon U–Pb isotopic analyses were conducted using laser ablation inductively coupled plasma mass spectrometry (LA–ICP–MS) at the Yuheng Mineral and Rock Laboratory, Kehui Testing (Tianjin) Technology Co., Ltd., Tianjin, China. The analytical system consisted of an Analytik Jena PQMS (Endress+Hauser, Jena, Germany) inductively coupled plasma mass spectrometer coupled with a RESOlution 193 nm excimer laser ablation system (Australian Scientific Instruments, Canberra, Australia). Analyses were performed in single-spot ablation mode with a laser spot diameter of 26 μm, a repetition rate of 5 Hz, and an energy density of approximately 5 J/cm^2. Helium (He) was used as the carrier gas, while argon (Ar) was employed as the make-up gas. The two gases were mixed through

a T-connector before entering the ICP. Each analytical cycle consisted of approximately 15–20 s of background signal acquisition followed by 45 s of signal acquisition from the ablated zircon. Zircon reference material GJ-1 was used as the primary reference material for U–Pb isotopic calibration. During analysis, two measurements of GJ-1 were performed after every 5–10 unknown analyses. Time-dependent instrumental drift in U–Th–Pb isotopic ratios was corrected by linear interpolation based on repeated measurements of GJ-1. The uncertainty associated with the recommended isotopic values of GJ-1 was propagated to the final analytical results. The Plešovice zircon reference material was periodically analyzed as an unknown sample to monitor analytical accuracy and instrumental stability. Its measured weighted mean $^{206}Pb/^{238}U$ age was 337.5 ± 1.6 Ma ($n = 15$, 2σ), which is consistent with its recommended value of 337.13 ± 0.37 Ma [20].

Elemental concentrations of U, Th, and Pb were calibrated using NIST SRM 610 silicate glass as the external standard, with Zr as the internal standard. Raw analytical data were processed using Iolite 4 software, including background subtraction, signal integration, time-dependent drift correction, and quantitative calibration. According to the laboratory analytical results, most analytical spots yielded $^{206}b/^{204}Pb$ ratios greater than 1000, indicating that the proportion of common Pb relative to radiogenic Pb was very low. Therefore, no common Pb correction was applied. Analyses exhibiting anomalously high ^{204}Pb signals, potentially resulting from mineral inclusions or common Pb contamination, were excluded from subsequent age calculations. The concordance of individual zircon analyses was evaluated by comparing the $^{206}Pb/^{238}U$ and $^{207}Pb/^{235}U$ ages. The percentage concordance was calculated as $C = (t_{68}/t_{75}) \times 100$, where t_{68} and t_{75} represent the $^{206}Pb/^{238}U$ and $^{207}Pb/^{235}U$ ages, respectively. Analyses with concordance values between 90% and 110% (corresponding to a relative age difference of ±10%) were retained for subsequent age interpretation [20,21]. Based on this criterion, 73 and 77 concordant analyses were retained from samples DWG-KP1 and DWG-KP5, respectively, yielding a total of 150 concordant ages. For age reporting, $^{207}Pb/^{206}Pb$ ages were adopted for zircon grains older than 1000 Ma, whereas $^{206}Pb/^{238}U$ ages were used for grains younger than 1000 Ma. All analytical uncertainties are reported at the 2σ level. Zircon U–Pb concordia diagrams and weighted mean ages were calculated and plotted using Isoplot 4.15 software.

3.2. Multidimensional Scaling (MDS) Analysis of Detrital Zircon Age Distributions

To quantitatively evaluate the similarities and differences among detrital zircon age distributions from different regions of the Tarim Basin and potential provenance areas, multidimensional scaling (MDS) analysis was employed. MDS is a multivariate ordination technique that transforms pairwise dissimilarities among multiple samples into a low-dimensional spatial configuration, thereby facilitating the simultaneous comparison and visualization of their relative affinities [22–24].

The MDS analysis in this study was primarily based on previously published detrital zircon U–Pb age data from potential source regions within and surrounding the Tarim Basin. The normalized age distribution functions of individual samples were integrated to obtain the corresponding cumulative distribution functions (CDFs). Following the K–S statistical approach proposed by Vermeesch [25], the maximum absolute vertical distance between the cumulative age distribution curves of two samples was calculated to quantify their pairwise dissimilarity. The calculation is expressed as follows:

$$D_{ij} = \max_{t} \left| F_i(t) - F_j(t) \right| \quad (1)$$

where D_{ij} represents the dissimilarity between samples i and j, and $F_i(t)$ and $F_j(t)$ denote the respective cumulative age distribution functions of the two samples. The pairwise dissimilarity values calculated for all samples were integrated into a symmetric dissimilarity

matrix, which was subsequently used as the input for two-dimensional MDS ordination. In the resulting MDS ordination, samples located closer to one another exhibit relatively similar detrital zircon age distribution characteristics. The relative spatial positions and clustering patterns of different samples were examined to further evaluate provenance affinities between potential source regions and sedimentary samples. It should be noted that the two dimensions of the MDS ordination (Dim1 and Dim2) have no intrinsic geological or geographical meaning; their interpretation is primarily based on the relative distances and spatial distribution patterns among samples [22–24].

The MDS analysis was employed as a supplementary quantitative tool for evaluating provenance similarity. Its results were interpreted comprehensively in conjunction with detrital zircon age distribution characteristics and regional geological settings, rather than being regarded as independent evidence for identifying specific provenance regions.

4. Results

4.1. Morphological Characteristics and Th/U Ratios of Detrital Zircons

Most zircon grains from sample DWG-KP1 exhibit well-defined oscillatory zoning, whereas a few grains display tabular morphologies (Figure 4). The zircon grains range mainly from 80 to 145 μm in size, with a predominant grain size of approximately 100 μm. Most grains are subangular, exhibiting relatively high euhedrality and well-preserved crystal forms, whereas only a few are subrounded or partially fractured. These morphological characteristics suggest that most zircon grains may have undergone moderate-distance sediment transport, whereas the more rounded grains may have experienced longer-distance transport or sedimentary recycling. The Th/U ratios of zircons from DWG-KP1 range from 0.13 to 2.75, with an average of 0.78, and all values exceed 0.1. Considering their crystal morphology, internal cathodoluminescence (CL) textures, and well-developed oscillatory zoning, the detrital zircons in sample DWG-KP1 are interpreted to be predominantly magmatic in origin.

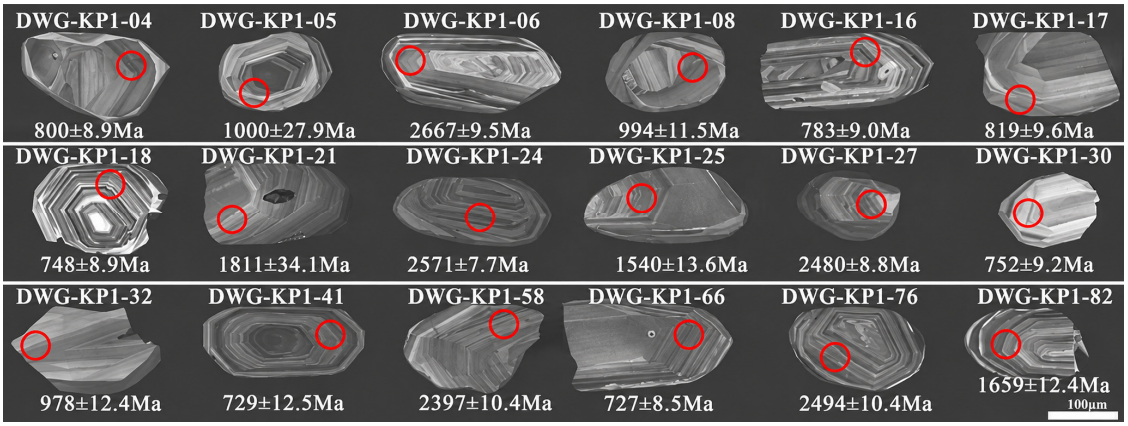


Figure 4. Cathodoluminescence (CL) images of representative zircon grains from sample DWG-KP1, showing analytical spots and corresponding U–Pb ages.

Zircon grains from sample DWG-KP5 generally exhibit well-defined oscillatory zoning (Figure 5), with grain sizes predominantly ranging from 100 to 130 μm. Most grains are subangular, with relatively high euhedrality and well-preserved crystal forms. These morphological characteristics suggest that most zircons may have undergone short- to moderate-distance sediment transport. The Th/U ratios range from 0.03 to 1.85, with an average of 0.74. Except for analysis DWG-KP5-57, all analytical spots yield Th/U ratios greater than 0.1. Based on combined evidence from crystal morphology, internal CL textures,

and oscillatory zoning, the detrital zircons from sample DWG-KP5 are also interpreted to be predominantly magmatic in origin.

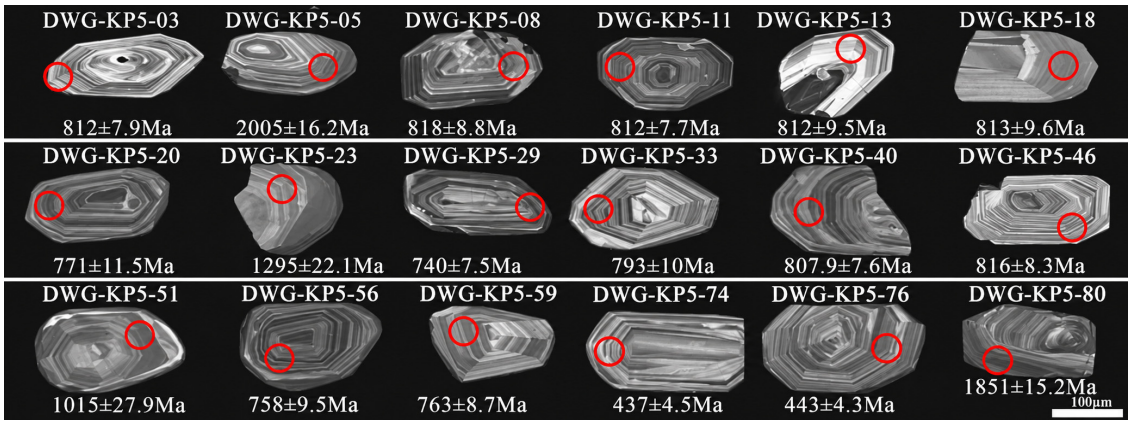


Figure 5. Cathodoluminescence (CL) images of representative zircon grains from sample DWG-KP5, showing analytical spots and corresponding U–Pb ages.

4.2. Trace Element Geochemistry of Detrital Zircons

The rare earth element (REE) compositions of detrital zircons from the lower and upper sandstone members of the Kepingtag Formation at the Dawangou section were normalized to chondritic values using the normalization parameters recommended by McDonough and Sun [26]. The normalized REE patterns are presented in Figures 6 and 7, and the corresponding trace element data are provided in the Supplementary Table S1.

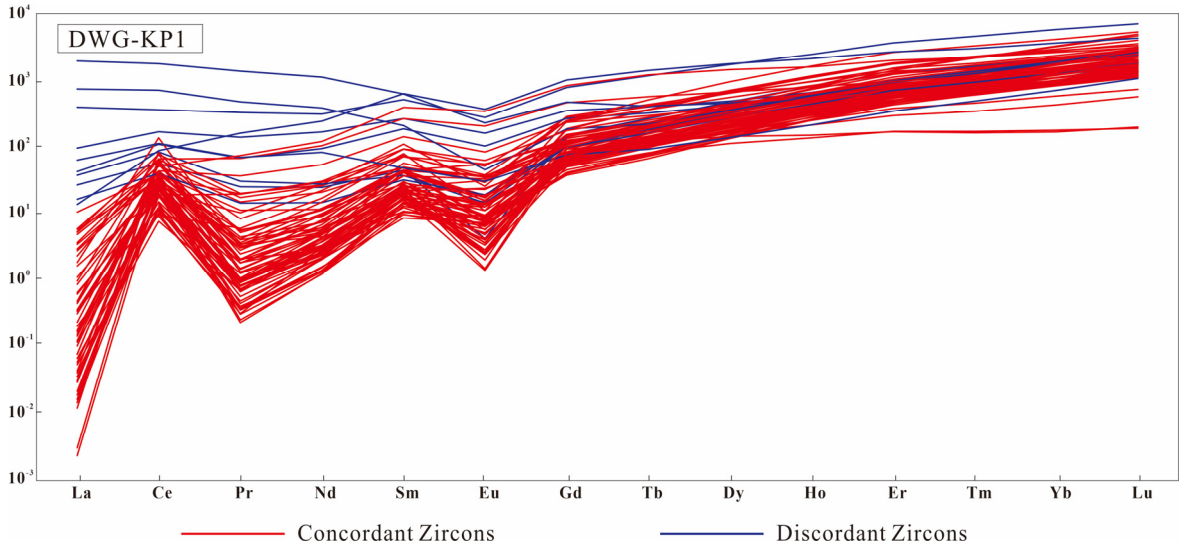


Figure 6. Chondrite-normalized REE patterns of zircons from sample DWG-KP1, Kepingtag Formation, Dawangou section, Tarim Basin.

The chondrite-normalized REE patterns of sample DWG-KP1 are generally characterized by steep right-sloping profiles, indicating relative depletion in light rare earth elements (LREEs) and pronounced enrichment in heavy rare earth elements (HREEs) (Figure 6). Most zircon grains exhibit positive Ce anomalies and distinct negative Eu anomalies. The Ce/Ce* values range from 1.10 to 1.57, whereas the Eu/Eu* values range from 0.018 to 0.735, with a mean of 0.283. A small proportion of zircon grains exhibit relatively elevated LREE abundances and comparatively weaker HREE fractionation. Based on the combined REE

distribution patterns, cathodoluminescence (CL) images, and Th/U ratios, the zircons in sample DWG-KP1 are interpreted to be predominantly of magmatic origin.

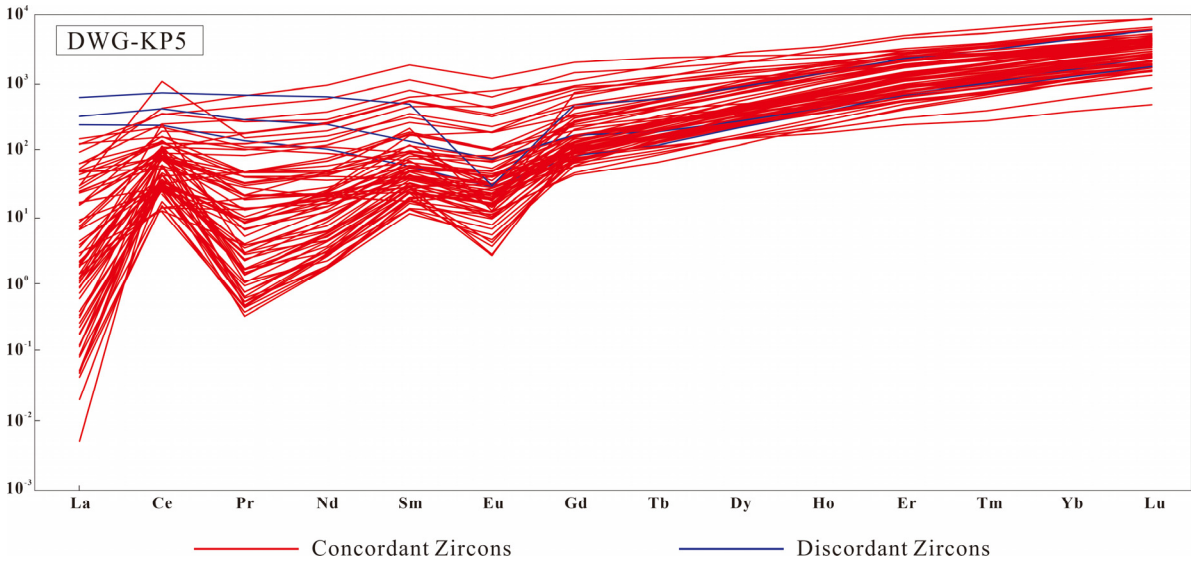


Figure 7. Chondrite-normalized REE patterns of zircons from sample DWG-KP5, Kepingtag Formation, Dawangou section, Tarim Basin.

Most zircon grains in sample DWG-KP5 exhibit REE geochemical characteristics typical of magmatic zircons, with chondrite-normalized patterns showing pronounced LREE depletion and HREE enrichment, forming steep right-sloping profiles (Figure 7). All concordant analyses exhibit positive Ce anomalies, with Ce/Ce* values ranging from 1.12 to 89.6. Eu displays distinct negative anomalies, with Eu/Eu* values ranging from 0.017 to 0.937 and a mean of 0.382. The exceptionally high Ce/Ce* values may be partly associated with very low La concentrations, potentially close to the analytical detection limit, which may amplify the calculated Ce anomalies. A small proportion of zircon grains exhibit relatively elevated LREE abundances and comparatively weaker HREE fractionation. Based on the combined characteristics of Ce and Eu anomalies, CL images, and Th/U ratios, the zircons in sample DWG-KP5 are interpreted to be predominantly of magmatic origin, whereas a few grains with atypical REE distribution patterns may record processes associated with deep-crustal material recycling or subsequent hydrothermal alteration.

4.3. Detrital Zircon U–Pb Age Distributions

A total of 164 zircon U–Pb analyses were conducted on two sandstone samples collected from the Kepingtag Formation at the Dawangou section. After excluding discordant analyses with concordance values below 90%, 150 concordant U–Pb ages were retained for further analysis. Analyses with concordance values below 90% were excluded from the relative frequency distributions. The complete analytical results are presented in the Supplementary Table S1. All analytical uncertainties reported in the Supplementary Table S1 and U–Pb concordia diagrams are expressed at the 2σ level. Unless otherwise specified, $^{207}Pb/^{206}Pb$ ages were adopted for zircon grains older than 1000 Ma, whereas $^{206}Pb/^{238}U$ ages were used for grains younger than 1000 Ma.

Of the 84 analytical spots analyzed from sample DWG-KP1, 73 yielded concordant U–Pb ages ranging from 706.7 ± 8.5 to 2667.4 ± 9.9 Ma. Among these, 29 ages are younger than 1000 Ma, ranging from 706.7 ± 8.5 to 999.2 ± 11.7 Ma and accounting for approximately 39.7% of the concordant ages. The remaining 44 analyses yielded $^{207}Pb/^{206}Pb$ ages older than 1000 Ma, ranging from 1000.3 ± 27.9 to 2667.4 ± 9.9 Ma. The age probability

distribution exhibits two prominent peaks at approximately 750 and 993.5 Ma, accompanied by two subordinate peaks at approximately 1850 and 2500 Ma (Figure 8). Overall, the detrital zircon age spectrum of the lower sandstone member of the Kepingtag Formation at the Dawangou section is dominated by ages between 700 and 1050 Ma, with a prominent Neoproterozoic age population.

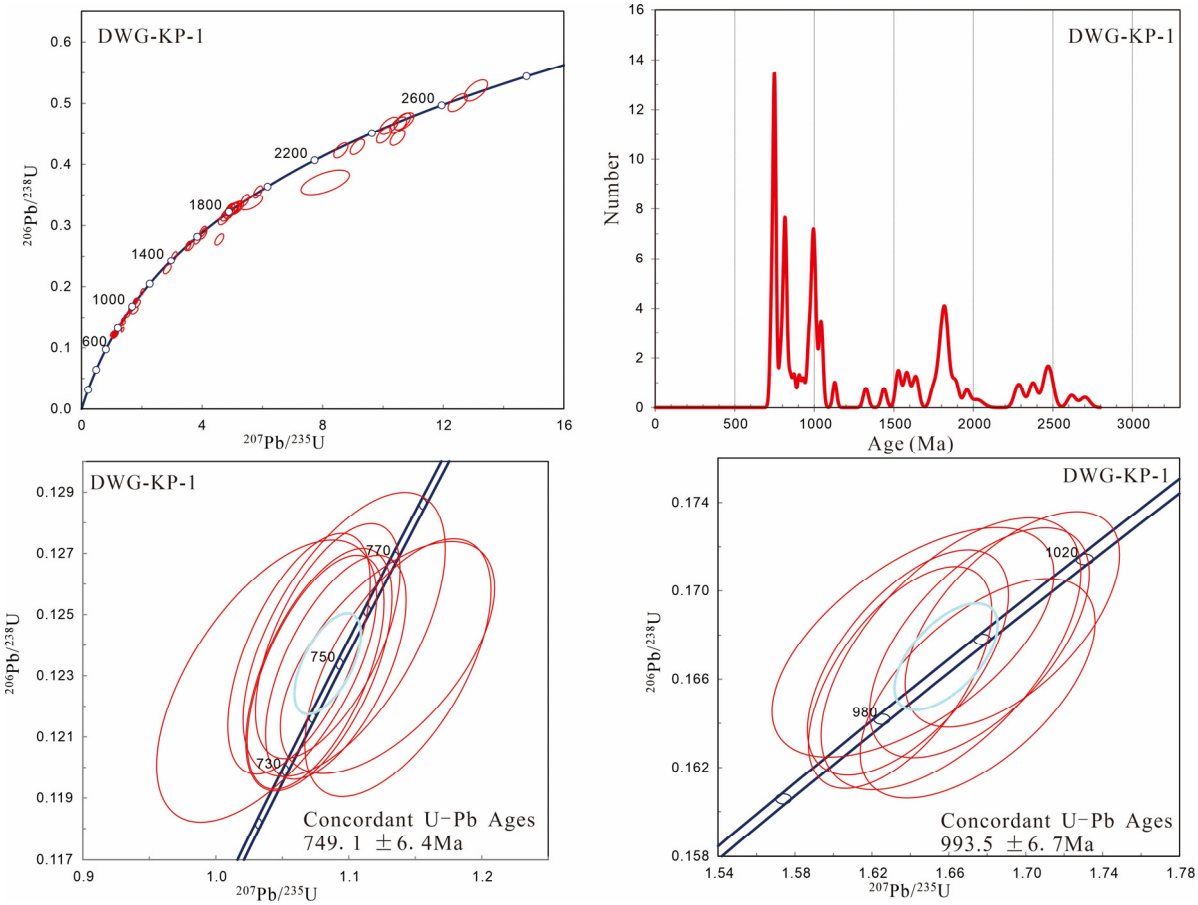


Figure 8. Zircon U–Pb concordia diagram and age distribution histogram for sample DWG-KP1 from the Silurian Kepingtag Formation, Tarim Basin.

Of the 80 analytical spots analyzed from sample DWG-KP5, 77 yielded concordant U–Pb ages ranging from 436.5 ± 4.5 to 2609.5 ± 18.4 Ma. Among these, 57 ages are younger than 1000 Ma, ranging from 436.5 ± 4.5 to 957.2 ± 8.8 Ma and accounting for approximately 74% of the concordant ages. The remaining 20 analyses yielded $^{207}Pb/^{206}Pb$ ages older than 1000 Ma, ranging from 1014.6 to 2609.5 Ma and representing approximately 26% of the concordant ages. The age probability distribution is characterized by two prominent peaks at approximately 761.5 ± 4.4 and 812.5 ± 3.7 Ma, together with a subordinate peak at approximately 440 Ma (Figure 9). Several additional minor peaks occur at approximately 950, 1600, 2000 and 2500 Ma. Overall, the detrital zircon age spectrum of the upper sandstone member is dominated by ages between 700 and 850 Ma, broadly consistent with the dominant age population of the lower sandstone member. Notably, sample DWG-KP5 also contains three younger zircon grains with U–Pb ages of 436.5 ± 4.5, 440.0 ± 4.8, and 443.2 ± 4.3 Ma.

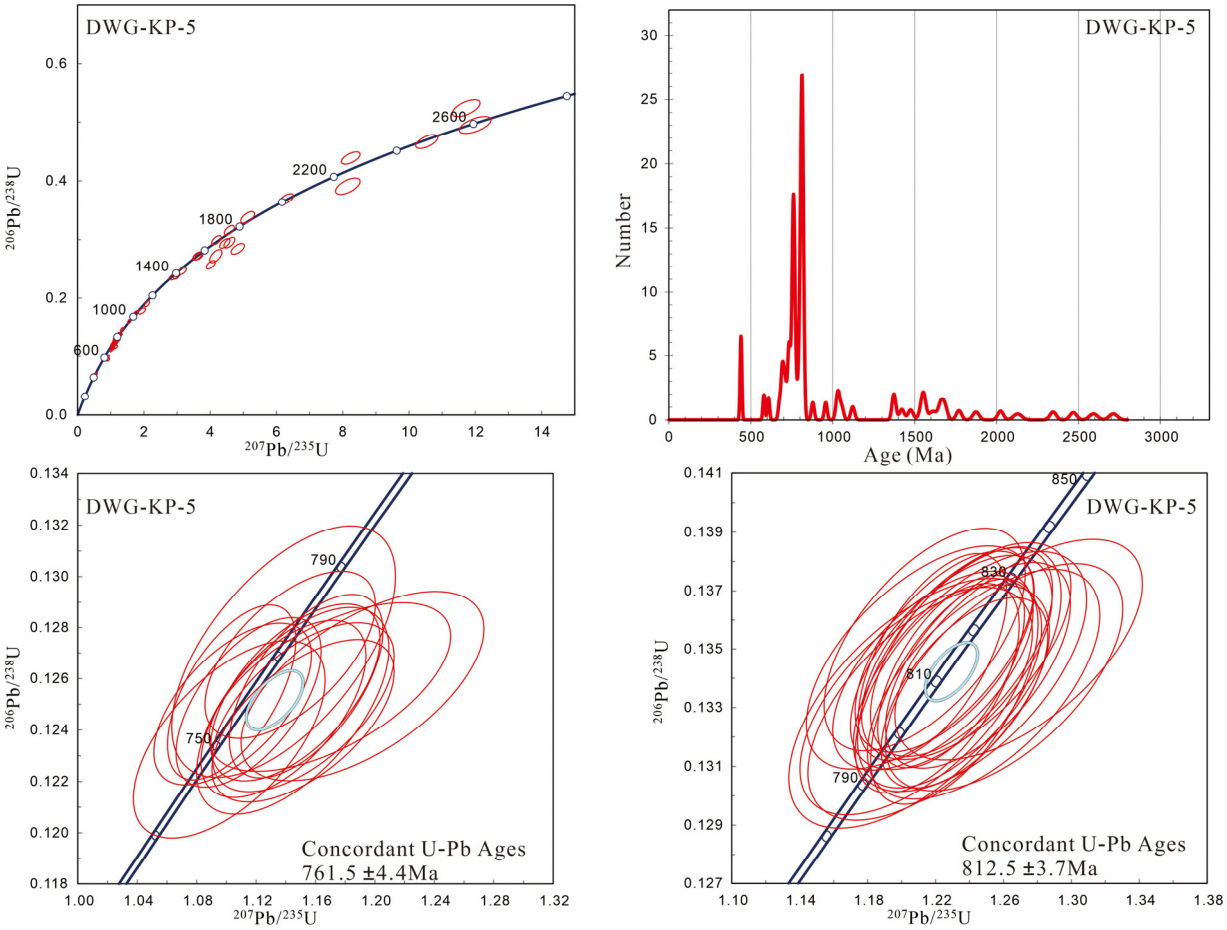


Figure 9. Zircon U–Pb concordia diagram and age distribution histogram for sample DWG-KP5 from the Silurian Kepingtag Formation, Tarim Basin.

5. Discussion

5.1. Identification of Potential Source Areas

During the Early Silurian, the Tarim Basin underwent significant tectonic reorganization associated with the Caledonian Orogeny, during which orogenic activity along the basin margins and differential tectonic movements of intracratonic paleo-uplifts jointly controlled the generation and transport of detrital material. By integrating the detrital zircon U–Pb age data obtained in this study with previously published geochronological data from the Precambrian basement of the Tarim Basin and its surrounding orogenic belts, a regional tectonic framework and detrital zircon age distribution map were compiled (Figure 10). Based on the detrital zircon age populations and the spatial distribution of potential source areas, the Silurian provenance systems of the Tarim Basin can be broadly classified into two categories characterized by distinct age ranges.

The first category comprises Early Paleozoic detrital sources derived from the surrounding orogenic belts. Early Paleozoic magmatic ages of approximately 500–400 Ma are widely recorded in tectonic belts along the northern, southern, and southeastern margins of the Tarim Basin. In the Altun region, magmatic ages are predominantly concentrated between approximately 500 and 450 Ma, whereas the West Kunlun Orogenic Belt and the southwestern basin margin contain abundant magmatic records ranging from approximately 455 to 430 Ma. Similarly, tectonic belts associated with the South Tianshan Orogenic Belt along the northern basin margin preserve Early Paleozoic age records of approximately 450–420 Ma. These age populations are broadly associated with Caledonian tectonic pro-

cesses, including oceanic lithosphere subduction, island-arc magmatism, and arc–continent collision. Subsequent uplift and erosion of the surrounding orogenic belts could have supplied relatively young igneous detritus to the basin. Therefore, the 500–400 Ma detrital zircon age population in the Kepingtag Formation may serve as an important provenance indicator of sediment input from the surrounding active orogenic belts, with a particularly strong correspondence between the eastern Tarim Basin and Early Paleozoic magmatic activity in the Altun Orogenic Belt.

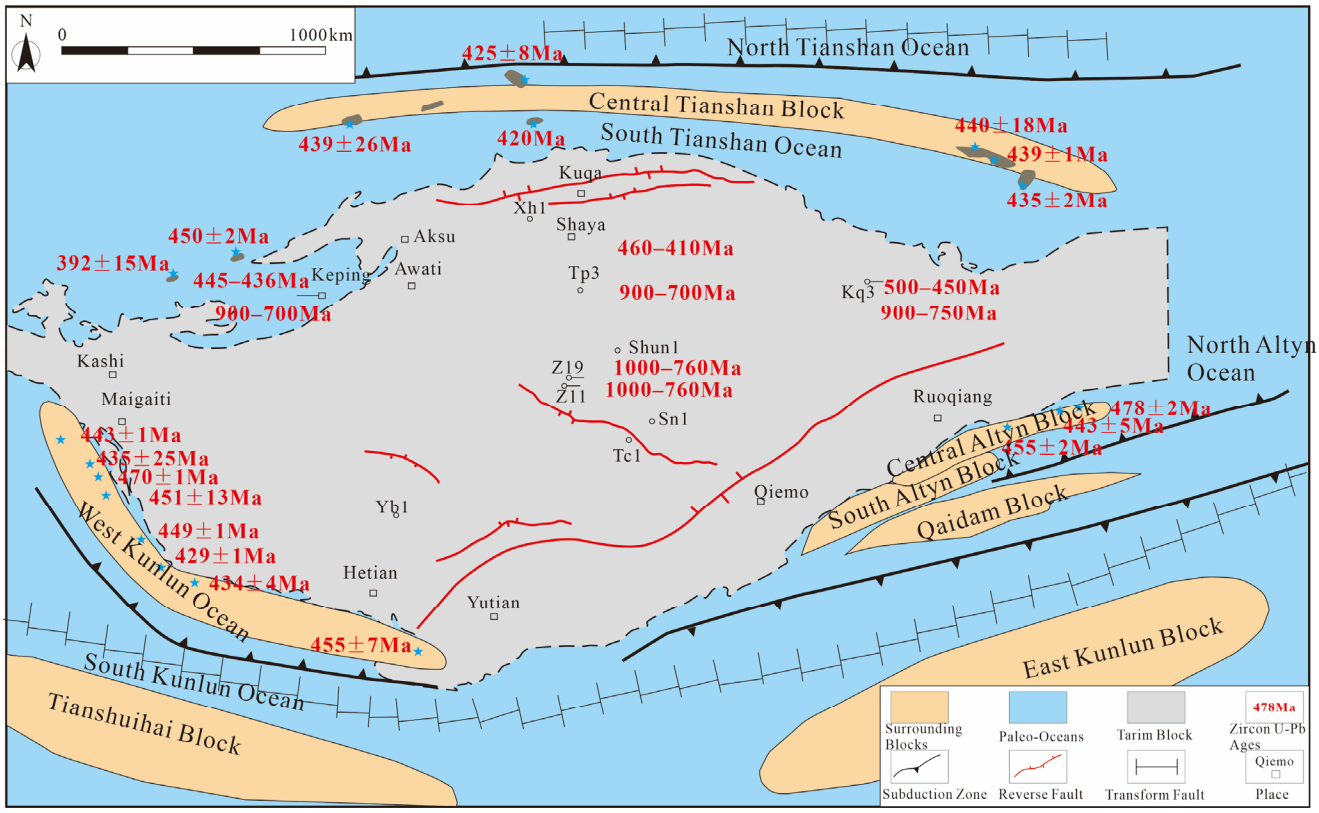


Figure 10. Regional tectonic setting and detrital zircon age distributions around the Tarim Basin during the third episode of the Middle Caledonian Orogeny. (Data sources: [27–31]).

The second category comprises inherited Neoproterozoic detrital sources derived from intracratonic and basin-margin paleo-uplifts. Neoproterozoic age populations of 1000–700 Ma, 900–700 Ma, and 900–750 Ma are widely preserved in the Tarim Craton and its surrounding paleo-uplifts, reflecting the persistent contribution of inherited Precambrian basement sources and associated paleo-uplifts to sediment supply.

Available data indicate that the basement of the Tarim Basin is not a homogeneous crystalline basement of a single age and composition, but rather a heterogeneous composite basement formed through multiple tectonothermal events, including Archean–Paleoproterozoic continental crust formation, Mesoproterozoic extension, Neoproterozoic convergence and amalgamation, and the breakup of the Rodinia supercontinent. Detrital zircon and basement igneous rock geochronological data from the Tarim Basin record several major Precambrian tectonothermal events at approximately 3100–2950 Ma, 2400–2100 Ma, 2000–1900 Ma, 1600–1300 Ma, 950–900 Ma, and 800–700 Ma (Figure 11). During the early to middle Neoproterozoic, the Tarim Block entered a stage of Rodinia supercontinent assembly and regional convergence, progressively developing a relatively coherent cratonic basement. At approximately 800–700 Ma, the tectonic regime of the Tarim Block gradually shifted from convergence to extension.

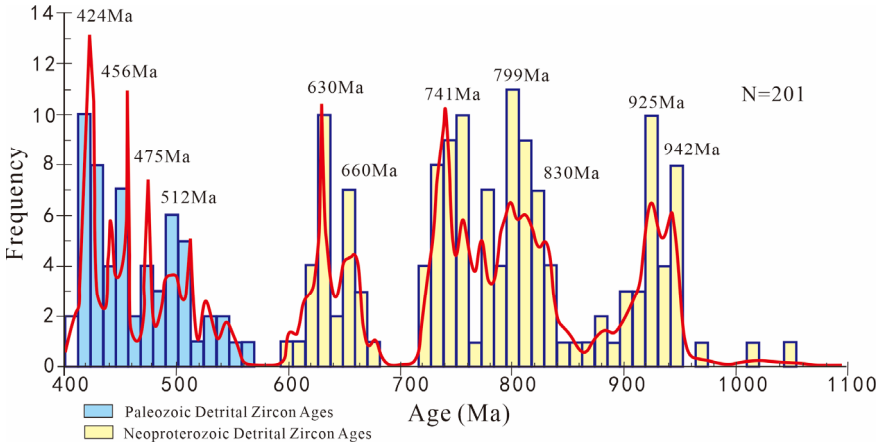


Figure 11. Histogram showing the U–Pb age distribution of Neoproterozoic–Early Paleozoic igneous rocks in the Tarim Craton (data compiled from [31–37]).

The pre-Silurian paleotectonic framework of the Tarim Basin developed through the superimposition of convergent orogenic processes along the basin margins since the Early–Middle Ordovician on a heterogeneous Precambrian basement. Since the end of the Early Ordovician, progressive subduction and closure of the peripheral Proto-Tethyan oceanic basins, particularly those associated with the West Kunlun and Altun orogenic belts, caused the Tarim Basin to gradually transition from a relatively stable Early Paleozoic cratonic platform setting to a compressional tectonic regime, accompanied by the reactivation of pre-existing basement highs. Regional paleotectonic studies indicate that varying degrees of uplift had occurred in the southwestern Tarim, Tazhong, Tabei, and Tadong regions by the end of the Early Ordovician. Subsequently, intense compression during the latest Ordovician resulted in large-scale uplift of the Tadong region, while the Tadongnan Uplift also became largely established. These tectonic events collectively formed several positive paleotopographic features within the basin prior to Silurian deposition [35–39]. A north–south-trending seismic profile across the basin reveals extensive uplift-related deformation and erosion, resulting in the development of regionally widespread angular and erosional unconformities (Figure 12).

In terms of their formation mechanisms, the Tabei, Tazhong, and Tadong uplifts are classified as basement-inherited paleo-uplifts. The Tabei Uplift had already developed prior to Cambrian deposition and experienced renewed folding and uplift during the Late Ordovician [40]. The Tazhong region was characterized by a pre-existing Precambrian basement high, although its Phanerozoic uplift primarily began during the latest Early Ordovician to Middle Ordovician. The Tadong Uplift also exhibits strong basement inheritance and underwent renewed, intense uplift during the Late Ordovician–Early Silurian in response to convergent compression associated with the Altun Orogenic Belt. Consequently, it became an important positive paleotopographic feature and potential sediment source area within the basin prior to Silurian deposition [41]. The Tadongnan Uplift was mainly formed during the Late Ordovician Caledonian tectonic event. Owing to its proximity to the Altun Orogenic Belt, this region experienced more intense compression, thrusting, and regional metamorphism during the Late Ordovician–Early Silurian. In contrast, the Southwestern Tarim Uplift exhibits characteristics of a foreland forebulge. This paleo-uplift began to develop at the end of the Middle Ordovician, underwent intensified uplift during the Late Ordovician, and continued to rise during the Silurian, rapidly extending eastward toward the Pishan–Hotan region. Tectonically, it is interpreted primarily as a forebulge associated with the Early Paleozoic West Kunlun foreland basin, and its eastward migra-

tion reflects the west-to-east propagation of orogenic deformation along the West Kunlun Orogenic Belt [39–42].

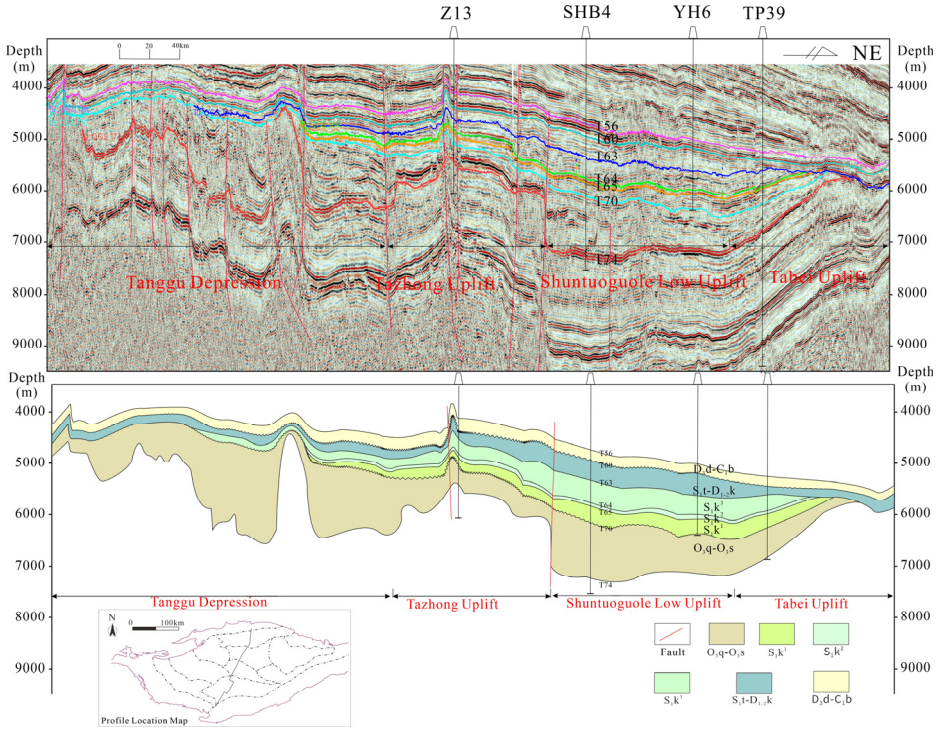


Figure 12. North–south-trending seismic–geological structural cross-section across the Tarim Basin from Well Z13 to Well TP39 (seismic data provided by the Northwest Oilfield Company, Sinopec).

In summary, the Tarim Basin was characterized by an overall uplift–depression configuration consisting of the Tabei Uplift–Central Depression–Southern Composite Paleo-uplift Belt–Tadong/Tadongnan Structural Highlands. Notably, the southern paleo-uplifts were unlikely to have been entirely isolated structural highs. Instead, they more likely constituted a segmented, composite positive paleotopographic belt formed through differential reactivation of the underlying southern Tarim basement during the Caledonian Orogeny [37,38,40–44]. Based on this tectonic framework, this study delineates the distribution of pre-depositional paleo-uplifts and potential sediment source areas within the Tarim Basin prior to deposition of the Kepingtag Formation, as illustrated in Figure 13.

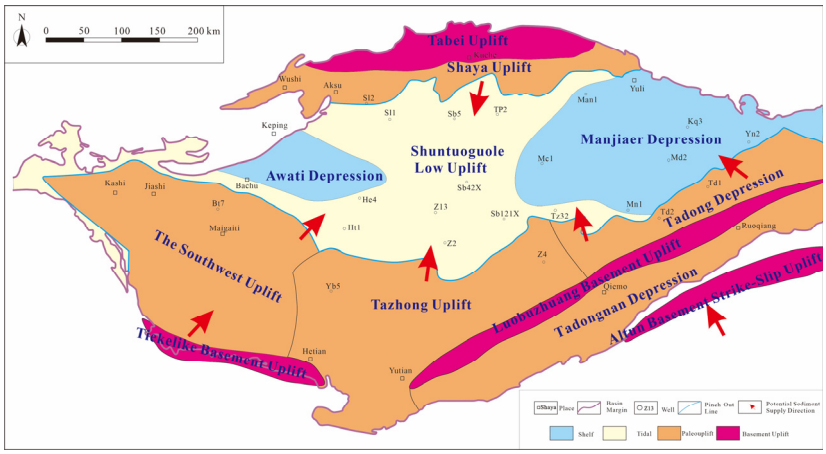


Figure 13. Schematic map showing the distribution of paleo-uplifts and potential sediment source areas within the Tarim Basin prior to deposition of the Kepingtag Formation.

5.2. Provenance Inheritance and Adjustment Between the Lower and Upper Sandstone Members of the Kepingtag Formation

The detrital zircon U–Pb age spectra of the Kepingtag Formation in the Tarim Basin exhibit distinct multimodal distributions, indicating contributions from both relatively young magmatic arcs and older basement rocks. Samples from different regions show variations in the positions and relative intensities of their major age peaks.

To minimize the limitations of provenance interpretations based on individual age peaks and facilitate consistent comparisons across different regions and stratigraphic members, the principal detrital zircon age populations were divided into three age clusters based on their age distribution characteristics: age cluster I (1100–700 Ma), age cluster II (2000–1600 Ma), and age cluster III (600–400 Ma). In addition to these three major age clusters, some samples contain ancient zircon grains older than 2000 Ma. However, these grains generally occur in relatively low proportions and exhibit scattered age distributions, without forming regionally persistent dominant peaks. Therefore, they are mainly regarded as supplementary evidence for contributions from ancient basement rocks.

Age cluster I (1100–700 Ma) is the most widely distributed age population across different regions of the Tarim Basin and its potential source areas, representing one of the most persistent detrital zircon age components in the Kepingtag Formation. This age interval is closely associated with Late Mesoproterozoic–Neoproterozoic tectonomagmatic activity in the Tarim Craton and is recorded to varying degrees in the Tabei basement and Precambrian rock assemblages of the Tiekelike, southwestern Tarim, Kuruktag, and Altun regions. These age records reflect Neoproterozoic crustal reservoirs formed and reworked during the assembly and breakup of the Rodinia supercontinent. Because this age signature is widely preserved in the Precambrian basement of the Tarim Craton and its Nanhua–Sinian (Cryogenian–Ediacaran) sedimentary cover, age cluster I primarily reflects sediment contributions from inherited intracratonic basement sources and recycled sedimentary successions [35,36,45–47].

Age cluster II (2000–1600 Ma) mainly records Paleoproterozoic continental crust formation, accretion, and subsequent reworking events within the Tarim Craton. This age population is commonly documented in Precambrian basement regions, including Tabei, southwestern Tarim, and Tiekelike. It shows a broad temporal correspondence with crustal accretion and reworking associated with the assembly of the Columbia supercontinent and therefore represents an important geochronological indicator of contributions from ancient cratonic basement rocks [33–36,46].

Age cluster III (600–400 Ma) is primarily associated with Caledonian tectonomagmatic events along the margins of the Tarim Basin. Early Paleozoic magmatic records are preserved to varying degrees in the Altun, Kuruktag, and West Kunlun regions, as well as in the active tectonic belts along the northern margin of the Tarim Basin. Compared with the two older age clusters, age cluster III provides a more direct geochronological indicator of Early Paleozoic orogenic activity [29–32] and generally suggests enhanced sediment input from the surrounding active orogenic belts or Early Paleozoic magmatic arcs.

On this basis, the following sections systematically examine the provenance characteristics of the lower and upper sandstone members of the Kepingtag Formation. By integrating multidimensional scaling (MDS) results, similarities and differences among detrital zircon age distributions from different regions are further evaluated to identify potential sediment source regions and explore their variations between the two depositional stages.

5.2.1. Comparison of Detrital Zircon U–Pb Age Spectra and Potential Source Areas in the Lower Sandstone Member

The detrital zircon U–Pb age spectra of the lower sandstone member of the Kepingtag Formation are generally dominated by Precambrian age populations. Age cluster I (1100–700 Ma) and age cluster II (2000–1600 Ma) can be regarded as the two principal regional age clusters, whereas age cluster III (600–400 Ma) generally represents a subordinate component but shows significant local enrichment in the eastern basin (Figure 14). The detrital zircon age spectra exhibit pronounced spatial variations among different regions, indicating that a multi-source provenance system jointly controlled by intracratonic paleo-uplifts and surrounding active orogenic belts had already developed during deposition of the lower sandstone member.

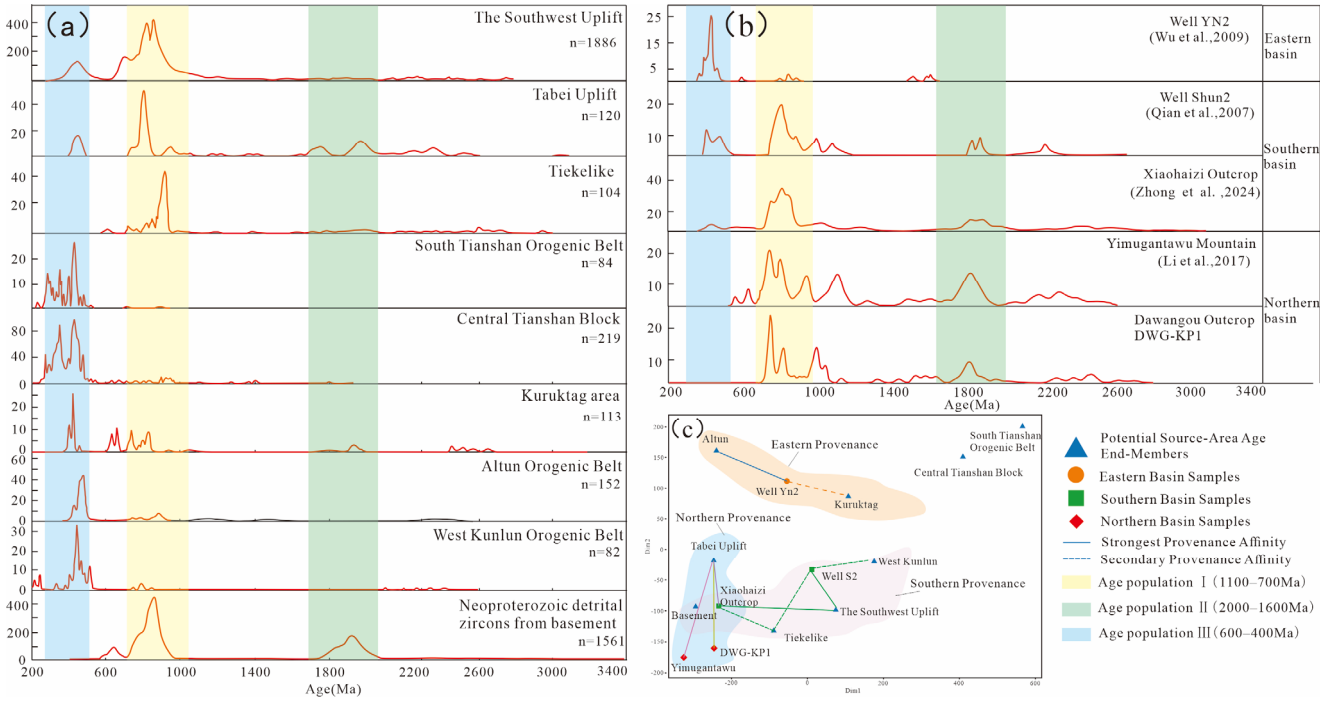


Figure 14. Comparison of detrital zircon U–Pb age spectra from the lower sandstone member of the Kepingtag Formation with those of potential source areas. (**a**) Detrital zircon age distributions of potential source areas surrounding the Tarim Basin; (**b**) detrital zircon U–Pb age distributions of samples from the lower sandstone member; (**c**) multidimensional scaling (MDS) plot of detrital zircon U–Pb age distributions. Data sources: [11,35,36,45–53].

In the eastern region, Well YN2 exhibits the most distinctive detrital zircon age spectrum compared with samples from other regions. It is characterized by a pronounced enrichment of the 600–400 Ma age cluster and relatively weak contributions from the 1100–700 Ma and 2000–1600 Ma age populations, indicating a dominant Early Paleozoic provenance signature. This age distribution corresponds well with the widespread Early Paleozoic island-arc and collisional magmatic activity in the Altun region. Integrating the differences in detrital zircon age distributions revealed by MDS analysis, the pronounced enrichment of younger zircon age populations in Well YN2 may reflect additional sediment input from active tectonic belts along the eastern margin of the Tarim Basin. In particular, rocks associated with Caledonian tectonomagmatic activity in the Altun Orogenic Belt may have constituted an important potential sediment source, while the Kuruktag region may also have contributed detrital material. Therefore, the lower sandstone member in the eastern basin already exhibits a distinct provenance signature controlled by surrounding orogenic belts, contrasting with the basement-dominated provenance systems in the basin interior.

In the southern region, the detrital zircon age spectra of Well S2 and the Xiaohaizi section are strongly dominated by the 1100–700 Ma age cluster, accompanied by a significant 2000–1600 Ma component and a minor population of 600–400 Ma zircons. The overall age spectrum of Well S2 shows a strong affinity with the Precambrian crustal reservoirs of the Southwestern Tarim Uplift and the Tiekelike region, suggesting that its principal sediment sources were derived from erosion of paleo-uplifts and recycling of Precambrian basement rocks and sedimentary cover sequences in southwestern Tarim. The minor Early Paleozoic zircon population may reflect additional contributions from Caledonian orogenic sources in the West Kunlun region. In contrast, the Xiaohaizi section exhibits a more pronounced mixed provenance signature. Its 1100–700 Ma and 2000–1600 Ma age populations are comparable to those of the Tabei Uplift and also show similarities to the Precambrian crustal reservoirs of the Tiekelike–Southwestern Tarim region. This interpretation is consistent with previous studies suggesting that the Tabei and Southwestern Tarim uplifts supplied detrital material to the Keping–Bachu region during the Late Ordovician–Early Silurian.

In the northern region, samples from Yimugantawu Mountain and Dawangou (DWG-KP1) are predominantly characterized by the 1100–700 Ma and 2000–1600 Ma age populations, whereas the 600–400 Ma age cluster is relatively weak. Their age spectra exhibit strong similarities to those of the Tabei Uplift and Neoproterozoic basement end-members of the Tarim Craton, suggesting that sediment supply to the northern basin during deposition of the lower sandstone member remained primarily dominated by erosion of pre-existing paleo-uplifts.

Overall, the provenance system during deposition of the lower sandstone member was dominated by inherited Precambrian basement sources within the Tarim Basin, with locally enhanced contributions from Caledonian orogenic sources in the eastern region. The 1100–700 Ma and 2000–1600 Ma age clusters constitute two persistent and regionally widespread age components, reflecting sustained sediment contributions from Late Mesoproterozoic–Neoproterozoic crustal reservoirs and Paleoproterozoic basement rocks, respectively. In contrast, the 600–400 Ma age cluster generally represents a subordinate component but becomes locally dominant in the eastern basin, indicating that Early Paleozoic active orogenic belts, particularly the Altun Orogenic Belt, had already contributed detrital material during the early stages of Kepingtag Formation deposition.

5.2.2. Comparison of Detrital Zircon U–Pb Age Spectra and Potential Source Areas in the Upper Sandstone Member

Compared with the lower sandstone member, the upper sandstone member retains a substantial contribution from Precambrian sources characterized by the 1100–700 Ma age population. However, the relative abundance of the 600–400 Ma age population increases markedly in the northern and eastern parts of the basin, whereas that of the 2000–1600 Ma age population generally decreases. Accordingly, age cluster I (1100–700 Ma) and age cluster III (600–400 Ma) can be regarded as the two principal age clusters during deposition of the upper sandstone member, while age cluster II (2000–1600 Ma) represents a subordinate contribution from ancient basement sources (Figure 15). The relatively young detrital zircon ages obtained from sample DWG-KP5 are broadly consistent with the timing of Early Silurian magmatic activity and provide additional constraints on the maximum depositional age of the upper sandstone member of the Kepingtag Formation, although they do not directly represent the actual depositional age of the sandstone [54,55]. Previous studies have also identified a few young detrital zircons with ages of approximately 437–435 Ma in the Kepingtag Formation of the Keping area, which were interpreted as potentially related to magmatic activity associated with subduction of the South Tianshan Ocean [52]. Furthermore, zircon U–Pb ages of 441.1 ± 4.2 Ma and 442.8 ± 2.4 Ma have been obtained

from arc-related gabbro and plagiogranite, respectively, in the South Tianshan region, providing further evidence for Early Silurian tectonomagmatic activity in this region [56]. These regional age records show a close temporal correspondence with the young detrital zircons in sample DWG-KP5, suggesting that these grains may have been derived from Early Paleozoic magmatic rocks along the basin margins and may reflect sediment contributions from sources associated with contemporaneous or near-contemporaneous tectonomagmatic activity during deposition of the Kepingtag Formation.

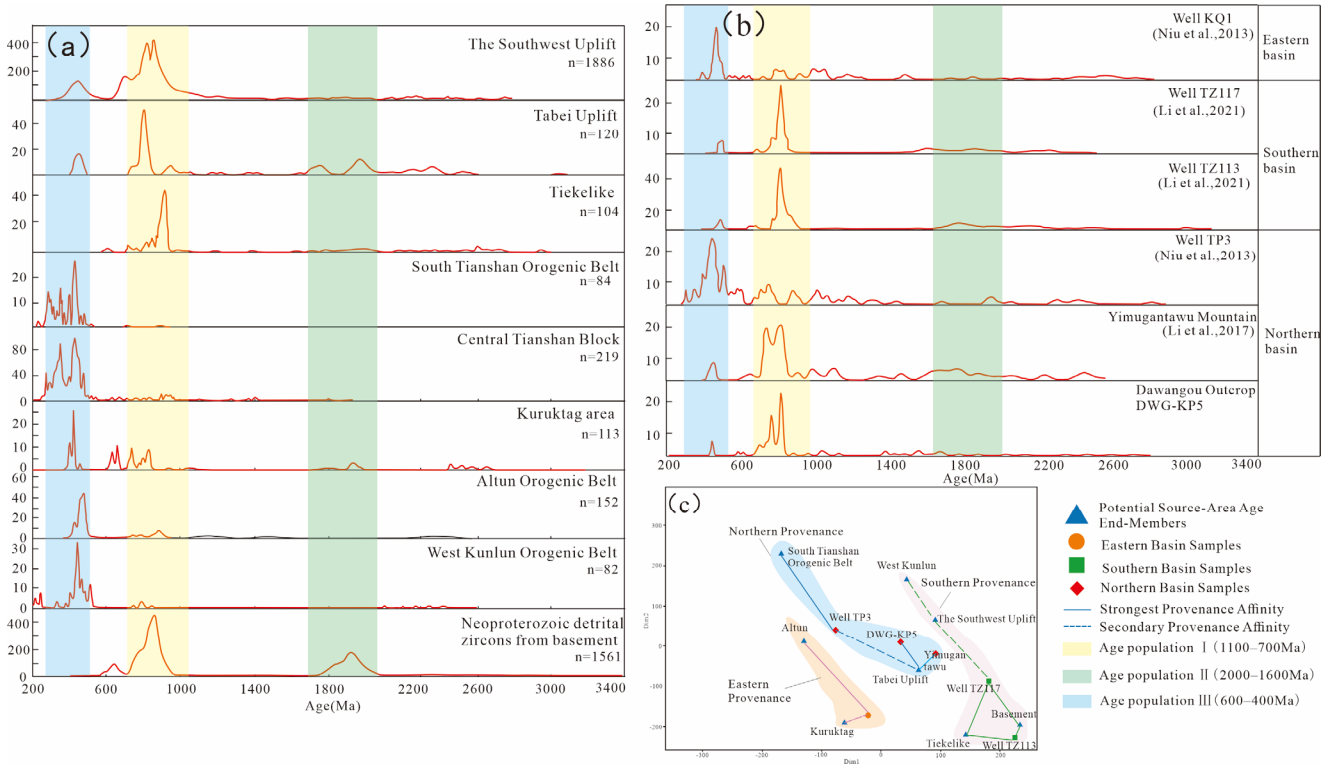


Figure 15. Comparison of detrital zircon U–Pb age spectra from the upper sandstone member of the Kepingtag Formation with those of potential source areas. (**a**) Detrital zircon age distributions of potential source areas surrounding the Tarim Basin; (**b**) detrital zircon U–Pb age distributions of samples from the upper sandstone member; (**c**) multidimensional scaling (MDS) plot of detrital zircon U–Pb age distributions. Data sources: [8,35,36,46–53].

In the eastern region, the detrital zircon age spectrum of Well KQ1 is characterized by a pronounced dominance of the 600–400 Ma age population, accompanied by a relatively minor 1100–700 Ma component. This distribution indicates that sediment supply to the eastern basin remained strongly influenced by Early Paleozoic active orogenic sources during deposition of the upper sandstone member. The Early Paleozoic magmatic zircons in Well KQ1 are interpreted to have been derived primarily from Caledonian magmatic and orogenic sources associated with the Altun Orogenic Belt. Therefore, provenance in the eastern basin maintained a strong affinity with active orogenic sources throughout deposition of both the lower and upper sandstone members.

In the southern region, Wells TZ117 and TZ113 exhibit a pronounced dominance of the 1100–700 Ma age cluster, with only minor contributions from the 600–400 Ma age population. Their detrital zircon age spectra correspond closely to the Precambrian age distributions of the Tiekelike–Southwestern Tarim region [9], indicating that the principal sediment sources in the southern basin remained largely unchanged during deposition of the upper sandstone member. Sediment supply continued to be dominated by erosion of Precambrian basement rocks and recycling of sedimentary cover sequences associated

with the Southwestern Tarim–Tiekelike region and related paleo-uplifts. The minor Early Paleozoic zircon population may reflect continued influence from the West Kunlun orogenic system, although its relative contribution was substantially lower than that of Precambrian sources. Thus, the southern provenance system exhibits strong vertical inheritance between the lower and upper sandstone members.

In the northern region, samples from Well TP3, Yimugantawu Mountain, and Dawangou (DWG-KP5) retain the prominent 1100–700 Ma Neoproterozoic age cluster but exhibit a marked increase in the 600–400 Ma age population relative to the lower sandstone member. This change suggests that, in addition to the inherited sediment supply from the Tabei Uplift, the northern basin received an increased contribution from Early Paleozoic active tectonic belts during deposition of the upper sandstone member. Considering the regional tectonic setting characterized by Early Paleozoic subduction–accretion processes associated with the South Tianshan Ocean and the development of locally active continental-margin conditions along the northern margin of the Tarim Basin [1], we propose that the increased proportion of younger detrital zircons in the northern upper sandstone member may reflect enhanced sediment input from northern active tectonic belts in response to intensified subduction–accretion processes associated with the South Tianshan Ocean. Within this provenance framework, the Tabei Uplift likely continued to supply Precambrian detritus characterized by the 1100–700 Ma age population, whereas the South Tianshan active tectonic belt may have represented an important potential source of the younger 600–400 Ma detrital zircon population. This suggests that the provenance system in the northern basin retained sediment contributions from ancient basement sources while potentially experiencing additional influences from surrounding active tectonic belts. The timing and polarity of subduction of the South Tianshan Ocean remain controversial. Earlier studies generally favored a model in which the South Tianshan oceanic lithosphere was subducted northward beneath the Yili–Central Tianshan Block, while the northern margin of the Tarim Basin remained a stable passive continental margin. However, increasing evidence supporting southward or bidirectional subduction of the South Tianshan Ocean has emerged in recent years. For example, numerous Paleozoic granitoid intrusions have been identified in the Kuruktag region. Zircon U–Pb dating yielded ages of 419.2 ± 3.1 Ma for the pluton southeast of Tiemenguan and 418 ± 2.7 Ma for the Bostengxiang pluton. These intrusions are characterized by calc-alkaline to high-K calc-alkaline I-type granites and exhibit geochemical signatures typical of volcanic-arc granites formed along convergent plate margins [57–59]. The occurrence and age distributions of these convergence-related granitoid intrusions, together with regional structural deformation and kinematic characteristics, are difficult to reconcile with a model involving exclusively northward subduction of the South Tianshan Ocean. These observations suggest that southward subduction may also have occurred, potentially resulting in a bidirectional subduction system [60–64].

In this study, Early Paleozoic detrital zircon age populations were identified in the upper sandstone member of the Kepingtag Formation at the Dawangou section in northwestern Tarim and in Well TP3 in the northern basin. These age populations are not prominently represented in the corresponding lower sandstone member samples, suggesting that sediment input from Early Paleozoic sources became more pronounced during the later stages of Kepingtag Formation deposition. In addition, published geochronological data from the southern margin of Central Tianshan and the northern margin of the Tarim Basin were compiled and statistically analyzed (Figure 16). Integrating the available geochronological evidence from ophiolites, high-pressure metamorphic rocks, and granitoids suggests that the collisional orogenic evolution of the South Tianshan Belt followed a diachronous, scissor-like collision process, characterized by earlier collision in the eastern segment and later collision in the western segment [47].

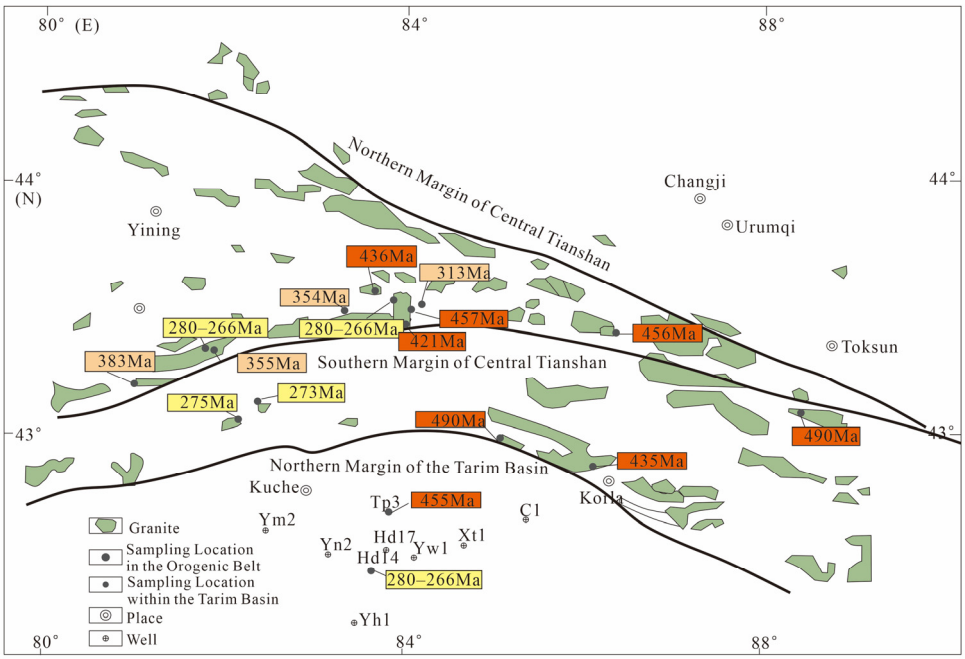


Figure 16. Schematic map showing the distribution of granitic rocks and geochronological dating results in the South Tianshan and along the northern margin of Central Tianshan. Base map modified from [47]; data sources: [15,57–67].

5.2.3. Integrated Provenance Constraints from Multiple Geological Indicators

Detrital zircon U–Pb geochronology provides valuable insights into the tectonothermal evolution of sediment source regions. However, variations in zircon fertility among different source rocks, together with the effects of hydraulic sorting during weathering, transport, and sedimentary recycling, mean that detrital zircon age distributions may not fully represent the overall provenance of sediments [68]. Therefore, integrating sandstone petrography, heavy mineral assemblages, and whole-rock geochemical characteristics can provide additional constraints on the source-rock compositions and provenance characteristics of the Kepingtag Formation.

Previous petrographic studies of the Kepingtag Formation along the northwestern margin of the Tarim Basin have shown that the sandstones are predominantly lithic quartz sandstones and lithic sandstones, with minor feldspathic lithic sandstones. The lithic fragments are mainly of igneous origin, accompanied by subordinate metamorphic and sedimentary rock fragments, indicating contributions from multiple source-rock types, particularly crystalline basement rocks and recycled sedimentary successions [69]. Whole-rock major and trace element analyses further indicate that the sandstones of the Kepingtag Formation are characterized by relatively high SiO_2 contents and low abundances of ferromagnesian components. Associated trace element ratios and rare earth element (REE) distribution patterns generally suggest substantial contributions from felsic igneous source rocks, together with evidence of sedimentary recycling [52].

Furthermore, Liu et al. identified a stable heavy mineral assemblage dominated by garnet, zircon, tourmaline, and rutile in the lower part of the Kepingtag Formation in the Tahe area [70]. Combined with regional sedimentological characteristics, their results suggest that the source rocks were predominantly Precambrian igneous and metamorphic rocks. By integrating heavy mineral assemblages and detrital zircon geochronological data from Paleozoic sandstones in the Keping area, Guo et al. further proposed that Silurian sediment supply was influenced not only by intracratonic paleo-uplifts but also potentially by surrounding orogenic belts [10].

Overall, the source-rock characteristics inferred from previous studies of sandstone detrital compositions, heavy mineral assemblages, and whole-rock geochemistry are broadly consistent with the provenance characteristics revealed by detrital zircon U–Pb geochronology in this study. Contributions from felsic igneous rocks, ancient crystalline basement rocks, and recycled sedimentary successions are compatible with the widespread 1100–700 Ma and 2000–1600 Ma zircon age populations in both the lower and upper sandstone members of the Kepingtag Formation. These independent lines of evidence collectively support persistent sediment supply from Precambrian basement rocks and inherited paleo-uplifts. Meanwhile, regional variations in the younger 600–400 Ma zircon population, particularly in the northern and eastern parts of the Tarim Basin, further suggest that Early Paleozoic orogenic activity along the basin margins exerted an additional influence on the pre-existing provenance system.

Nevertheless, given the limited number of newly analyzed sandstone samples and the relatively small number of young detrital zircon grains, the proposed provenance inheritance and stage-dependent adjustments should be regarded as interpretations supported by the available geochronological and regional geological evidence, rather than definitive reconstructions of regional provenance evolution, and require further validation through additional sampling and independent provenance indicators.

5.3. Effects of Tectonic Activity and Changes in Paleogeomorphic Configuration on Provenance

The Late Ordovician–Early Silurian tectonic framework and detrital zircon age spectra indicate that the provenance system of the lower sandstone member of the Kepingtag Formation was characterized by pronounced tectonic compartmentalization and a dual-source provenance signature. Caledonian orogenic activity along the basin margins not only directly supplied relatively young Early Paleozoic detritus represented by the 600–400 Ma age population but also promoted the reactivation of inherited paleo-uplifts, including the Tabei, Tazhong, and Tadong uplifts, through regional compression. Consequently, Precambrian basement rocks and recycled sedimentary cover sequences became important sediment sources. The eastern basin was most strongly influenced by orogenic activity in the Altun region, as indicated by the pronounced enrichment of 600–400 Ma detrital zircons, forming a composite provenance system dominated by the active orogenic belt and the Tadong Uplift. In contrast, the southern basin was primarily controlled by Precambrian basement uplifts in the southern Tarim, Tazhong, and southwestern Tarim regions, with sediment contributions dominated by the 1100–700 Ma and 2000–1600 Ma age populations, accompanied by minor Caledonian detritus derived from the West Kunlun Orogenic Belt. The northern basin was predominantly supplied by Precambrian materials derived from the inherited Tabei Uplift, whereas Early Paleozoic sediment contributions from the South Tianshan region remained relatively limited. Therefore, provenance during deposition of the lower sandstone member was jointly controlled by Late Ordovician–Early Silurian peripheral orogenic activity, differential uplift of intracratonic paleo-uplifts, and the regional uplift–depression configuration (Figure 17).

During deposition of the upper sandstone member, marine transgression associated with the middle mudstone member and subsequent paleogeomorphic reorganization resulted in the progressive submergence of some relatively low-relief paleo-uplifts, including parts of the Tazhong Uplift [41,47,51], thereby weakening sediment supply from proximal sources. Meanwhile, continued subduction–accretion and orogenic activity along the South Tianshan and Altun orogenic belts increased the relative contribution of detrital material from active tectonic belts to the northern and eastern regions of the basin. In contrast, sediment supply to the southern basin remained predominantly controlled by Precambrian basement sources in the Tiekelike region (Figure 18). These observations suggest that,

although the upper sandstone member largely inherited the provenance framework established during deposition of the lower sandstone member, continued peripheral orogenic activity and marine transgression induced stage-dependent adjustments in provenance composition and paleogeomorphic configuration. This evolution was characterized by the persistent contribution of inherited Precambrian basement sources, accompanied by enhanced Early Paleozoic detrital input from active tectonic belts in the northern and eastern regions of the basin.

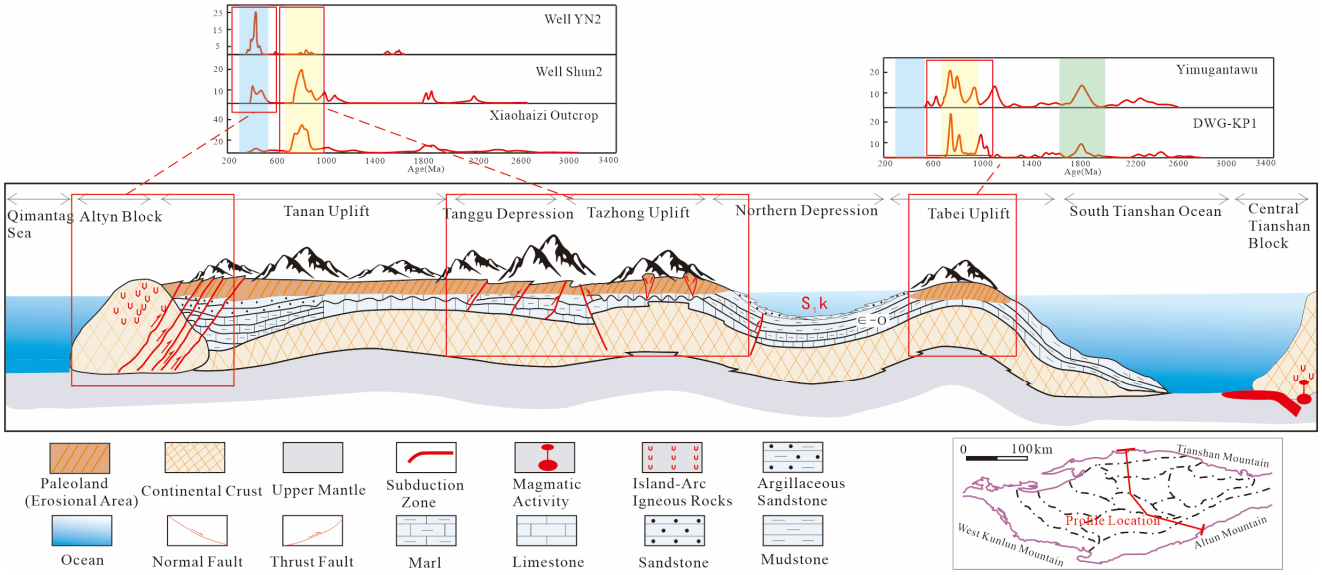


Figure 17. Schematic diagram of stratigraphic architecture and sediment provenance of the lower sandstone member of the Kepingtag Formation in the Tarim Basin.

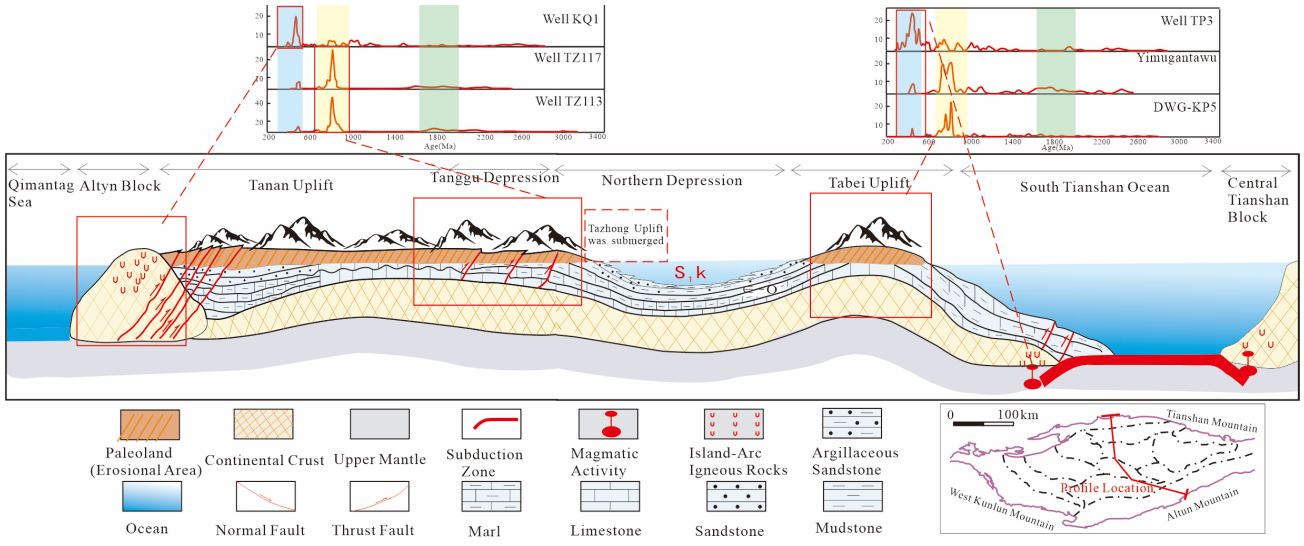


Figure 18. Schematic diagram of stratigraphic architecture and sediment provenance of the upper sandstone member of the Kepingtag Formation in the Tarim Basin.

6. Conclusions

Based on newly obtained detrital Zircon U–Pb geochronological data from the Dawangou section, together with previously published detrital zircon age distributions and regional tectonic and paleogeomorphic evidence, this study systematically investigated provenance

inheritance and adjustment between the lower and upper sandstone members of the Early Silurian Kepingtag Formation in the Tarim Basin. The principal conclusions are as follows:

(1) Detrital zircon U–Pb geochronological analyses of two sandstone samples collected from the Dawangou section yielded a total of 150 concordant ages. The lower sandstone member (DWG-KP1) is characterized by two prominent age peaks at approximately 750 and 994 Ma, accompanied by subordinate Paleoproterozoic and Neoarchean age populations. The upper sandstone member (DWG-KP5) remains dominated by Neoproterozoic age populations, with major peaks at approximately 762 and 813 Ma, but also contains three relatively young detrital zircon grains with ages of 443.2 ± 4.3, 440.0 ± 4.8, and 436.5 ± 4.5 Ma. These results indicate substantial inheritance of Neoproterozoic detrital components between the lower and upper sandstone members at Dawangou, together with the appearance of an Early Paleozoic detrital zircon age signature in the upper sandstone member.

(2) Regional comparisons of detrital zircon age spectra identified three characteristic age populations: 1100–700 Ma (cluster I), 2000–1600 Ma (cluster II), and 600–400 Ma (cluster III). The lower sandstone member is generally dominated by two Precambrian age populations, clusters I and II, whereas cluster III is relatively minor but becomes locally prominent in eastern Tarim. In the upper sandstone member, cluster I remains widely distributed, while cluster III becomes more prominent in northern and eastern Tarim, and the relative contribution of cluster II generally decreases. These variations indicate that provenance evolution of the Kepingtag Formation did not involve a complete replacement of pre-existing sediment sources. Instead, the relative contributions of ancient basement sources and Early Paleozoic orogenic sources changed against a background of continuous sediment supply from inherited basement sources.

(3) During deposition of the lower sandstone member, inherited intracratonic and basin-margin paleo-uplifts constituted the principal sediment sources. In the northern region, sediments were predominantly derived from Precambrian basement rocks and recycled sedimentary successions associated with the Tabei Uplift, whereas the southern region mainly received detrital material from the Precambrian basement and related paleo-uplifts of the Tiekelike–Southwestern Tarim region. In contrast, the eastern region exhibited a pronounced Early Paleozoic provenance signature, consistent with sediment supply from the Altun Orogenic Belt and associated structural highs in eastern Tarim. This spatial distribution indicates that a regionally differentiated provenance system, jointly controlled by the reactivation of inherited paleo-uplifts and peripheral orogenic activity, had already developed during deposition of the lower sandstone member. During deposition of the upper sandstone member, the overall provenance framework remained largely inherited but underwent regionally differentiated adjustments. In eastern Tarim, the continued enrichment of Early Paleozoic detrital zircon populations indicates the persistent influence of the Altun orogenic system on sediment supply. In southern Tarim, Neoproterozoic age populations remained dominant, reflecting continued sediment contributions from the Tiekelike–Southwestern Tarim region. In contrast, the northern region exhibited a more pronounced Early Paleozoic detrital zircon component superimposed on the inherited Precambrian age signature. This change is consistent with enhanced sediment input from active tectonic belts along the northern margin of the Tarim Basin and may be associated with the subduction–accretion evolution of the South Tianshan Ocean. Nevertheless, the contributions of individual Early Paleozoic source regions remain difficult to distinguish unequivocally and require further constraints from additional provenance indicators.

(4) Provenance inheritance and adjustment in the Kepingtag Formation were jointly influenced by peripheral orogenic activity, differential reactivation of intracratonic paleo-

uplifts, and changes in basin paleogeography. During the early depositional stage, sediment supply was primarily controlled by exposed Precambrian basement paleo-uplifts and their recycled sedimentary cover sequences. With subsequent marine transgression and paleogeomorphic reorganization, direct sediment supply from some low-relief intracratonic paleo-uplifts may have decreased, while continued tectonic activity along the basin margins enhanced the relative influence of peripheral orogenic sources in northern and eastern Tarim. Therefore, provenance evolution of the Kepingtag Formation was characterized by stage-dependent adjustments driven by tectonic activity and paleogeographic changes superimposed on a persistent inherited Precambrian provenance framework.

Supplementary Materials: The following supporting information can be downloaded at: https://www.mdpi.com/article/10.3390/min16111191/s1. Supplementary Table S1: Statistical table of detrital zircon ages and trace element data.

Author Contributions: Conceptualization, X.Z. and J.T.; methodology, Q.Z. and X.Z.; software, Q.Z.; validation, Q.Z.; formal analysis, Q.Z.; investigation, Q.Z.; resources, Q.Z.; data curation, Q.Z.; writing—original draft preparation, Q.Z.; writing—review and editing, Q.Z.; visualization, Q.Z.; supervision, X.Z.; project administration, J.T.; funding acquisition, J.T. All authors have read and agreed to the published version of the manuscript.

Funding: This work was supported by the National Natural Science Foundation of China. The project title is "Study on multi-event depositional coupling and depositional process of lacustrine basin in continental depression: a case study of Chang 7-Chang 6 oil formation in Yanchang Triassic, Ordos Basin" [grant number 42372141].

Data Availability Statement: All underlying data supporting this study are available in the Supplementary Material.

Acknowledgments: We sincerely thank the anonymous reviewers and editors for their constructive comments, which have greatly improved the quality of this manuscript.

Conflicts of Interest: The authors declare no conflicts of interest.

References

1. Lin, C.S.; Li, H.; Liu, J.Y. Major unconformities, tectonostratigraphic frameword, and evolution of the superimposed Tarim Basin, Northwest China. *J. Earth Sci.* **2012**, *23*, 395–407. [CrossRef]
2. Zhang, C.L.; Zou, H.B.; Li, H.K.; Wang, H.Y. Tectonic framework and evolution of the Tarim Block in NW China. *Gondwana Res.* **2013**, *23*, 1306–1315. [CrossRef]
3. He, B.; Jiao, C.; Xu, Z.; Cai, Z.; Zhang, J.; Liu, S.; Li, H.; Chen, W.; Yu, Z. The paleotectonic and paleogeography reconstructions of the Tarim Basin and its adjacent areas (NW China) during the late Early and Middle Paleozoic. *Gondwana Res.* **2016**, *30*, 191–206. [CrossRef]
4. Shi, K.; Liu, B.; Jiang, W.; Gao, X.; Liu, S.; Shen, Y. Sedimentary and evolutionary characteristics of Sinian in the Tarim Basin. *Pet. Res.* **2017**, *2*, 264–280. [CrossRef]
5. Yuan, H.; Chen, S.; Dai, K.; Guo, X.; Kong, L.; Feng, N.; Zhao, H.; Yang, W. Distribution of Cambrian source rock controlled by the inherited paleotopography on the Precambrian basement in the Tarim Basin, NW China. *Front. Earth Sci.* **2022**, *10*, 864082. [CrossRef]
6. Zhang, L.Q.; Li, Z.X.; Luo, X.R. Sedimentary-diagenetic characteristics and heterogeneity models of sandstone reservoirs: An example of Silurian Kalpintage Formation, Northwestern Tarim Basin, China. *Mar. Pet. Geol.* **2020**, *118*, 104440. [CrossRef]
7. Wang, S.Y.; Zhang, X.; Tian, J.C.; Peng, M.H.; Zheng, X.Y.; Xia, Y.T. Sedimentary evolution and sedimentary differentiation model of Kepingtag Formation in Shunbei area, Tarim Basin. *Lithol. Reserv.* **2021**, *33*, 81–94.
8. Niu, L.; Yu, B.S.; Zhang, W.B. Provenance analysis and dating of parent rocks of the sandstones from Kepingtag Formation (Silurian) in the northern Tarim Basin. *Acta Sedimentol. Sin.* **2013**, *31*, 421–429.
9. Li, X.Q.; Ding, H.K.; Peng, P.; Wu, M.L.; Zhong, C.H.; Chai, X.; Liu, G.W.; Peng, L. Provenance of Silurian Kepingtag Formation in Tazhong area, Tarim Basin: Evidence from detrital zircon U-Pb geochronology. *Earth Sci.* **2021**, *46*, 2819–2831.

10. Guo, C.T.; Gao, J.; Li, Z. Driving mechanism of tectonic evolution in key Paleozoic period in Tarim Basin: Constraints from tracing of provenance attributes in Keping area. *Earth Sci.* **2024**, *49*, 4112–4129.
11. Zhong, Z.Q.; Hou, G.T.; Xia, J.K.; Li, X.; Wei, L.Y.; Chang, H.N. Detrital zircon U-Pb geochronology of Ordovician-Silurian strata in the northwestern platform of the Tarim Basin: Implications for provenance systems and tectonic evolution. *Gondwana Res.* **2024**, *134*, 1–20. [CrossRef]
12. Zhong, Z.Q.; Xia, J.K.; Huang, S.Y.; Luo, C.M.; Chang, H.N.; Li, X.; Wei, L.Y.; Zhang, H. Reconstruction of proto-type basin and tectono-paleogeography of Tarim block in early Paleozoic. *Front. Earth Sci.* **2023**, *11*, 1101360. [CrossRef]
13. Zhang, C.L.; Li, H.K. The Tarim Craton in the Northwest of China. *Int. Geol. Rev.* **2023**, *65*, 607–643. [CrossRef]
14. Lei, X.X.; Lin, C.S.; Liu, Y.F.; Pan, W.Q.; Li, H.; Zhang, M.L. Depositional systems, sediment dispersal and controlling factors of intracratonic basin fills, Early Silurian, Tarim Basin, Northwest China. *Geol. J.* **2026**, 1–23. [CrossRef]
15. Lin, C.S.; Yang, H.J.; Liu, J.Y.; Rui, Z.F.; Cai, Z.Z.; Zhu, Y.F. Distribution and erosion of the Paleozoic tectonic unconformities in the Tarim Basin, Northwest China: Significance for the evolution of paleo-uplifts and tectonic geography during deformation. *J. Asian Earth Sci.* **2012**, *46*, 1–19. [CrossRef]
16. Liu, H.; Lin, C.S.; Wang, Y.M.; Zhang, D.S. Temporal and spatial evolution analysis: The early Paleozoic paleo-uplifts in the Tarim Basin. *J. Earth Sci.* **2012**, *23*, 559–581. [CrossRef]
17. Wang, T.F.; Jin, Z.K.; Shi, Z.W.; Dai, X.C.; Cheng, R.H. Phanerozoic plate history and structural evolution of the Tarim Basin, northwestern China. *Int. Geol. Rev.* **2020**, *62*, 1555–1569. [CrossRef]
18. Zhu, H.; Zhang, X.; Tian, J.C.; Zhang, Q.Y.; Hao, J.L.; Zhu, Z.D.; Zhou, X.Y. Sedimentary facies distribution and evolutionary model of the Lower Silurian Kepingtag Formation in northern Tarim. *Mineral. Petrol.* **2025**, *46*, 169–185.
19. Li, B.; Zhang, H.B.; Xia, Q.S.; Peng, J.; Guo, Q. Quantitative evaluation of tight sandstone reservoir based on diagenetic facies—A case of Lower Silurian Kepingtage Formation in Shuntuoguole Low Uplift, Tarim Basin, China. *Front. Earth Sci.* **2021**, *8*, 597535. [CrossRef]
20. Sláma, J.; Košler, J.; Condon, D.J.; Crowley, J.L.; Gerdes, A.; Hanchar, J.M.; Horstwood, M.S.A.; Morris, G.A.; Nasdala, L.; Norberg, N.; et al. Plešovice zircon—A new natural reference material for U–Pb and Hf isotopic microanalysis. *Chem. Geol.* **2008**, *249*, 1–35. [CrossRef]
21. Spencer, C.J.; Kirkland, C.L.; Taylor, R.J.M. Strategies towards statistically robust interpretations of in situ U–Pb zircon geochronology. *Geosci. Front.* **2016**, *7*, 581–589. [CrossRef]
22. Vermeesch, P. Multi-sample comparison of detrital age distributions. *Chem. Geol.* **2013**, *341*, 140–146. [CrossRef]
23. Vermeesch, P.; Resentini, A.; Garzanti, E. An R package for statistical provenance analysis. *Sediment. Geol.* **2016**, *336*, 14–25. [CrossRef]
24. Ortega-Flores, B.; Solari, L.A.; Martini, M. Multidimensional scaling (MDS): A quantitative approximation of zircon ages to sedimentary provenance with some examples from Mexico. *J. South Am. Earth Sci.* **2021**, *110*, 103347. [CrossRef]
25. Vermeesch, P. Dissimilarity measures in detrital geochronology. *Earth Sci. Rev.* **2018**, *178*, 310–321. [CrossRef]
26. McDonough, W.F.; Sun, S.S. The composition of the Earth. *Chem. Geol.* **1995**, *120*, 223–253. [CrossRef]
27. Shi, R.D.; Yang, J.S.; Wu, C.L.; Wooden, J.L. First SHRIMP dating for the formation of the Late Sinian Yushigou ophiolite, North Qilian Mountains. *Acta Geol. Sin.* **2004**, *78*, 649–657.
28. Tian, Y.Z.; Yang, J.S.; Liu, F.; Zhao, Y.J.; Feng, G.Y.; Niu, X.L.; Zhang, L.; Gao, J. Petrological characteristics of Bulusitai gabbro and its constraint to the time of South Tianshan ocean subduction. *Acta Petrol. Sin.* **2014**, *30*, 2363–2380.
29. Wang, C.; Liu, L.; He, S.P.; Yang, W.Q.; Cao, Y.T.; Zhu, X.H.; Li, R.S. Early Paleozoic magmatism in west Kunlun: Constraints from geochemical and zircon U-Pb-Hf isotopic studies of the Bulong granite. *Chin. J. Geol.* **2013**, *48*, 997–1014.
30. Klemd, R.; Gao, J.; Li, J.L.; Meyer, M. Metamorphic evolution of (ultra)-high-pressure subduction-related transient crust in the South Tianshan Orogen (Central Asian Orogenic Belt): Geodynamic implications. *Gondwana Res.* **2015**, *28*, 1–25. [CrossRef]
31. Guo, R.H.; Hu, X.M.; Garzanti, E.; Lai, W.; Yan, B.; Mark, C. How faithfully do the geochronological and geochemical signatures of detrital zircon, titanite, rutile and monazite record magmatic and metamorphic events? A case study from the Himalaya and Tibet. *Earth Sci. Rev.* **2020**, *201*, 103082. [CrossRef]
32. Cao, Z.C.; Jiang, H.S.; Zhang, J.C.; Geng, F.; Sha, X.G.; Hao, J.L.; Li, T.; Guo, X.W.; Tao, Z. Structure and evolution of Precambrian basement in southwestern Tarim Basin. *Pet. Geol. Exp.* **2023**, *45*, 844–856.
33. Xu, Z.Q.; He, B.Z.; Zhang, C.L.; Zhang, J.X.; Wang, Z.M.; Cai, Z.H. Tectonic framework and crustal evolution of the Precambrian basement of the Tarim Block in NW China: New geochronological evidence from deep drilling samples. *Precambrian Res.* **2013**, *235*, 150–162. [CrossRef]
34. Zhang, J.X.; Zhang, Z.M.; Xu, Z.Q.; Yang, J.S.; Cui, J.W. Petrology and geochronology of eclogites from the western segment of the Altyn Tagh, northwestern China. *Lithos* **2001**, *56*, 187–206. [CrossRef]
35. Gao, Z.; Fan, T. Intra-platform tectono-sedimentary response to geodynamic transition along the margin of the Tarim Basin, NW China. *J. Asian Earth Sci.* **2014**, *96*, 178–193. [CrossRef]

36. Li, Z.; Qiu, N.S.; Chang, J.; Yang, X.M. Precambrian evolution of the Tarim Block and its tectonic affinity to other major continental blocks in China: New clues from U–Pb geochronology and Lu–Hf isotopes of detrital zircons. *Precambrian Res.* **2015**, *270*, 1–21. [CrossRef]
37. Tang, L.J.; Huang, T.Z.; Qiu, H.J.; Wan, G.M.; Li, M.; Yang, Y.; Xie, D.Q.; Chen, G. Fault systems and their mechanisms of the formation and distribution of the Tarim Basin, NW China. *J. Earth Sci.* **2014**, *25*, 169–182. [CrossRef]
38. Yang, X.; Xu, X.H.; Qian, Y.X.; Chen, Q.L.; Chu, C.L.; Jiang, H.J. Discussion on regional differences of basement composition of the Tarim Basin, NW China. *Geotecton. Metallog.* **2014**, *38*, 544–556.
39. He, B.Z.; Jiao, C.L.; Xu, Z.Q.; Cai, Z.H.; Liu, S.L.; Zhang, J.X.; Li, H.B.; Zhang, M. Distribution and migration of the Phanerozoic palaeo-uplifts in the Tarim Basin, NW China. *Earth Sci. Front.* **2015**, *22*, 277–289.
40. Ma, D.B.; Yang, M.; Du, D.D.; Wang, S.; Chen, J.J.; He, D.F.; Dong, H.K. Analysis of the superposition process of multiphase active paleo-uplift: Taking the Lunnan paleo-uplift in the Tarim Basin as an example. *Acta Petrol. Sin.* **2020**, *36*, 3523–3536. [CrossRef]
41. Yan, J.K.; Chen, H.L.; Cheng, X.G.; Chen, Y.Q.; Zeng, C.M.; Chen, C.; Wu, H.X. Migration of paleo-uplift in southwestern Tarim Basin and its implications for orogenesis and reservoir development, NW China. *Pet. Explor. Dev.* **2023**, *50*, 99–110. [CrossRef]
42. Wu, G.H.; Yang, H.J.; Qu, T.L.; Li, H.W.; Luo, C.S.; Li, B.L. The fault system characteristics and its controlling roles on marine carbonate hydrocarbon in the Central uplift, Tarim basin. *Acta Petrol. Sin.* **2012**, *28*, 793–805.
43. Wang, Q.; Li, S.Z.; Zhao, S.J.; Mu, D.L.; Guo, R.H.; Somerville, I. Early Paleozoic Tarim Orocline: Insights from paleogeography and tectonic evolution in the Tarim Basin. *Geol. J.* **2017**, *52*, 436–448. [CrossRef]
44. Liu, H.; Somerville, I.D.; Lin, C.S.; Zuo, S.J. Distribution of Palaeozoic tectonic superimposed unconformities in the Tarim Basin, NW China: Significance for the evolution of palaeogeomorphology and sedimentary response. *Geol. J.* **2016**, *51*, 627–651. [CrossRef]
45. Wu, G.H.; Zhang, B.S.; Guo, C.L.; Wang, C.L.; Gao, H. Detrital zircon U-Pb dating for the Silurian in northern Tarim Basin and its significance. *Geotecton. Metallog.* **2009**, *33*, 418–426.
46. Zhu, G.Y.; Liu, W.; Wu, G.H.; Ma, B.S.; Nance, R.D.; Wang, Z.C.; Xiao, Y.; Chen, Z.Y. Geochemistry and U-Pb-Hf detrital zircon geochronology of metamorphic rocks in terranes of the West Kunlun Orogen: Protracted subduction in the northernmost Proto-Tethys Ocean. *Precambrian Res.* **2021**, *363*, 106344. [CrossRef]
47. Liu, J.Y.; Yang, H.J.; Yang, Y.H.; Cai, Z.Z.; Liu, Y.Q.; Rui, Z.F.; Su, Z.Z. The U-Pb chronologic evidence and sedimentary responses of Silurian tectonic activities at northeastern margin of Tarim Basin. *China Earth Sci.* **2012**, *55*, 1445–1460. [CrossRef]
48. Long, X.P.; Yuan, C.; Sun, M.; Zhao, G.C.; Xiao, W.J.; Wang, Y.J.; Yang, Y.H.; Hu, A.Q. Archean crustal evolution of the northern Tarim craton, NW China: Zircon U-Pb and Hf isotopic constraints. *Precambrian Res.* **2010**, *180*, 272–284. [CrossRef]
49. Liu, J.Y.; Lin, C.S.; Li, S.T.; Cai, Z.Z.; Xia, S.Q.; Fu, C.; Liu, Y.Q. Detrital zircon U–Pb geochronology and its provenance implications on Silurian Tarim basin. *J. Earth Sci.* **2012**, *23*, 455–475. [CrossRef]
50. Zhang, C.G.; Liu, L.; Wang, Z.W.; Li, D.; Wang, Y.L.; Ma, X.C.; Tang, W.Y.; Zhao, J.X.; Wang, F.; Chen, H.D. Permian source-to-sink processes and paleogeographic reconstruction in the northern Ordos Basin and its surrounding areas. *Acta Sedimentol. Sin.* **2025**, *43*, 1605–1624.
51. Qian, Y.X.; He, Z.L.; Cai, X.Y.; Zhang, J.T. Characteristics of and U-Pb ages of zircons and its implication from zircon of Donghe sandstones of the upper Devonian and Silurian sandstones in Tazhong area, Tarim basin. *Acta Petrol. Sin.* **2007**, *23*, 3003–3014.
52. Li, L.L.; Yang, B.Z.; Yin, Y.H.; Liu, L.L.; Wang, B. Provenance analysis from Early Silurian Kepingtag Formation in Keping Area, Xinjiang: Constraints from geochemical characteristics and zircon U-Pb geochronology. *Geol. Sci. Technol. Inf.* **2017**, *36*, 1–12.
53. Zhang, C.L.; Li, H.K.; Santosh, M.; Li, Z.X.; Zou, H.B.; Wang, H.Y.; Ye, H.M. Precambrian evolution and cratonization of the Tarim Block, NW China: Petrology, geochemistry, Nd-isotopes and U–Pb zircon geochronology from Archaean gabbro-TTG–potassic granite suite and Paleoproterozoic metamorphic belt. *J. Asian Earth Sci.* **2012**, *47*, 5–20. [CrossRef]
54. Dickinson, W.R.; Gehrels, G.E. Use of U–Pb ages of detrital zircons to infer maximum depositional ages of strata: A test against a Colorado Plateau Mesozoic database. *Earth Planet. Sci. Lett.* **2009**, *288*, 115–125. [CrossRef]
55. Coutts, D.S.; Matthews, W.A.; Hubbard, S.M. Assessment of widely used methods to derive depositional ages from detrital zircon populations. *Geosci. Front.* **2019**, *10*, 1421–1435. [CrossRef]
56. Wang, X.S.; Klemd, R.; Gao, J.; Jiang, T.; Li, J.L.; Xue, S.C. Final assembly of the southwestern Central Asian Orogenic Belt as constrained by the evolution of the South Tianshan Orogen: Links with Gondwana and Pangea. *Geophys. Res. Solid Earth* **2018**, *123*, 7361–7388. [CrossRef]
57. Guo, R.Q.; Qin, Q.; Muhetaer, Z.; Zhao, L.L.; Sun, M.J.; Wei, Z. Geological characteristics and tectonic significance of Ordovician granite intrusions in the western segment of Quruqtagh, Xinjiang. *Earth Sci. Front.* **2013**, *20*, 251–263.
58. Jahn, B.M.; Windley, B.F.; Natal'in, B.A.; Dobretsov, N.L. Phanerozoic continental growth in Central Asia. *Asian Earth Sci.* **2004**, *23*, 599–603. [CrossRef]
59. Ge, R.F.; Zhu, W.B.; Wilde, S.A.; He, J.W.; Cui, X.; Wang, X.; Bihai, Z. Neoproterozoic to Paleozoic long-lived accretionary orogeny in the northern Tarim Craton. *Tectonics* **2014**, *33*, 302–329. [CrossRef]

60. Rogers, J.J.W.; Santosh, M. Tectonics and surface effects of the supercontinent Columbia. *Gondwana Res.* **2009**, *15*, 373–380. [CrossRef]
61. Han, B.F.; He, G.Q.; Wang, X.C.; Guo, Z.J. Late Carboniferous collision between the Tarim and Kazakhstan–Yili terranes in the western segment of the South Tian Shan Orogen, Central Asia, and implications for the Northern Xinjiang, western China. *Earth Sci. Rev.* **2011**, *109*, 74–93. [CrossRef]
62. Xiao, W.J.; Windley, B.F.; Allen, M.B.; Han, C.M. Paleozoic multiple accretionary and collisional tectonics of the Chinese Tianshan orogenic collage. *Gondwana Res.* **2013**, *23*, 1316–1341. [CrossRef]
63. Wang, B.; Shu, L.S.; Faure, M.; Jahn, B.M.; Cluzel, D.; Charvet, J.; Chung, S.L.; Meffre, S. Paleozoic tectonics of the southern Chinese Tianshan: Insights from structural, chronological and geochemical studies of the Heiyingshan ophiolitic mélange (NW China). *Tectonophysics* **2011**, *497*, 85–104. [CrossRef]
64. Yang, T.N.; Li, J.Y.; Sun, G.H.; Wang, Y.B. Earlier Devonian active continental arc in Central Tianshan: Evidence of geochemical analyses and zircon SHRIMP dating on mylonitized granitic rock. *Acta Petrol. Sin.* **2006**, *22*, 41–48.
65. Zhu, Z.X.; Li, J.Y.; Dong, L.H.; Zhang, X.F.; Wang, K.Z.; Wang, H.X.; Zhao, T.Y. Tectonic framework and tectonic evolution of the southern Tianshan, Xinjiang, China. *Geol. Bull. China* **2009**, *28*, 1863–1870.
66. Zhu, Y.F.; Zhang, L.F.; Gu, L.B.; Guo, X.; Zhou, J. The zircon SHRIMP chronology and trace element geochemistry of the Carboniferous volcanic rocks in western Tianshan Mountains. *Chin. Sci. Bull.* **2005**, *50*, 2201–2212. [CrossRef]
67. Liu, C.X.; Xu, B.L.; Zou, T.R.; Lu, F.X.; Tong, Y.; Cai, J.H. Petrochemistry and tectonic significance of Hercynian alkaline rocks along the northern margin of the Tarim Platform and its adjacent area. *Xinjiang Geol.* **2004**, *22*, 43–49.
68. Chew, D.; O'Sullivan, G.; Caracciolo, L.; Mark, C.; Tyrrell, S. Sourcing the sand: Accessory mineral fertility, analytical and other biases in detrital U–Pb provenance analysis. *Earth Sci. Rev.* **2020**, *202*, 103093. [CrossRef]
69. Zhang, Q.Y.; Tian, J.C.; Zhang, X.; Hao, S.Y.; Li, Z.P.; Ji, K. Provenance analysis of the Silurian Kepingtag Formation in the northwest margin of Tarim Basin—Evidence from petrology and geochemistry. *Minerals* **2025**, *15*, 934. [CrossRef]
70. Liu, R.H.; Wang, M.; Jiang, Z.X.; Yang, W.L. Development of sedimentary facies type in Silurian lower Kepingtage Formation, Tahe area. *Acta Sedimentol. Sin.* **2016**, *34*, 326–335.

Disclaimer/Publisher's Note: The statements, opinions and data contained in all publications are solely those of the individual author(s) and contributor(s) and not of MDPI and/or the editor(s). MDPI and/or the editor(s) disclaim responsibility for any injury to people or property resulting from any ideas, methods, instructions or products referred to in the content.